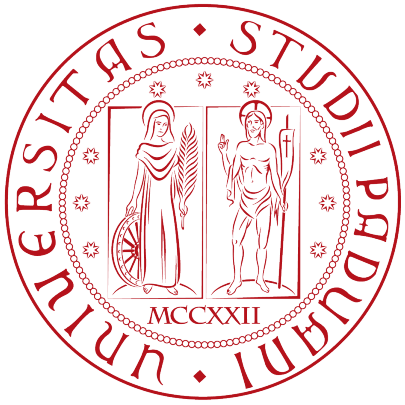

Università degli Studi di Padova

Dipartimento di Matematica
"Tullio Levi–Civita"

Corso di Laurea Magistrale in Matematica

DYNAMIC MONGE-KANTOROVICH MODELING OF BLOOD VESSEL NETWORKS

RELATORE
Ch.mo Prof. Mario Putti

CORRELATORE
Dott. Enrico Facca
Dott. Caterina De Bacco

LAUREANDO
Marco Cibin
1138184

22 Febbraio 2019

Anno Accademico 2018/2019

Contents

Introduction

In this thesis we are studying a biological application of the Optimal Transport Problem: we would like to investigate on a possible link between Branched Transport Problem and the theoretical results obtained by a number of biologists in the last century about the structure of arterial networks. These biological results were highly appreciated in the 20th century biological literature and some models based on them are still used in current studies. The scope of this thesis is to correlate these studies with the modern theory of Branched Transport, starting from the dynamical Monge-Kantorovich problem reported in [12], [13] and [14].
In 1926 ([23]) the biologist Murray speculated that the structure of an arterial network could be obtain by the minimization of a cost function formed by two addends: the first one is related to a Poiseuille flow on a cylinder, while the other one represents the cost of the network. Later, after having found a direct relationship between the flow and the cube of the radius of the cylinder, the so-called "Murray's Law", he managed to compute the measure of an angle at a bifurcation point. Murray's results seemed to be confirmed by empirical data, so a number of authors developed his ideas during the second part of the last century. They generalized Murray's model considering more general kinds of flow and cost functions.
On the other hand, the first mathematical formulation of the Optimal Transport Problem can be found in a work of 1781 by Monge ([21]). The idea is to determine how to move with minimal transportation costs some material from a starting configuration to a final one. Monge's ideas were developed during the last century so that more general situations could be considered, such as those ones in which a concentration of mass is penalized or favored. This last case is called Branched Transport Problem.
In [12], [13] and [14] a dynamic formulation of OTP and BTP was proposed. In [13] the authors conjecture that this formulation is equivalent to the Monge-Kantorovich formulation and in [14] they report an efficient, accurate and robust numerical solver. In [1] this formulation has been proposed for the numerical solution of branched transport problems, and several nu-

merical experiments shows its efficacy and robustness. For these reason, we use this dynamic formulation to reconstruct an arterial network. Then we compare our results with the theoretical biological laws based on Murray's ideas.

The structure of this thesis is as follows.

In Chapter 1 we are introducing the theory of Optimal Transport, starting from the first formulation by Monge in [21]. Different formulations of this problem in both discrete and continuous cases are presented. Lastly, we discuss about different equivalent formulations of branched problem.

In Chapter 2 we give a historical review about the biological results on arteries networks and their branching angles. The starting point of this discussion is the work of 1926 by Murray [23]. A number of authors decided to develop its theory and we are going to report the main results which leaded to the generalization of Murray's hypothesis of having a Poiseuille flow of blood. Lastly, after having reported the theoretical measure for the bifurcation angles, depending only on the geometry of the system and on the properties of the blood flow, we show an equivalence between these angles and the measure of the bifurcation angles of the branched transport theory.

In Chapter 3 we introduce a numerical approach that allow the solution of the Optimal Transport Problem, as described in [12]. There is a proof of the connection between Dynamic Monge-Kantorovich Model and Optimal Transport Problem, but the proof of a similar link for the Branched Problem has not been found yet, even if there are many numerical evidences that seem to support the existence of this connection. Here we discuss both Dynamic Monge-Kantorovich Model and its discretization.

Lastly, in Chapter 4 we show some numerical applications of the ideas of the previous chapters. We would like to use the model described in Chapter 3 in order to obtain the arterial network of a frog tongue [9]. In this last chapter, after having shown explicitly the relation between the "biological" angles found in Chapter 2 and the exponent β of the Extended Dynamic Monge-Kantorovich Model of Chapter 3, we describe all the intermediate steps that let us analyze the bifurcation angles of the system, starting from the solution of the model. Then we proceed to analyze solutions obtained with different exponents β.

Chapter 1

Optimal Transport Problem

In this chapter we briefly introduce the Optimal Transport Problem (OTP) from historical and mathematical point of views. We first describe the original L^1 transport of Monge as extended by Kantorovich. Then we focus our discussion on the more recent Branched (or Ramified) transport. The material of this chapter is mostly taken from [3], [4], [12] and [28].

1.1 Monge Problem

The first mathematical formulation of the OTP can be found in a work by Gaspard Monge in 1781 [21]. It was based on a problem of military fortification construction. The problem was to determine how to move optimally some material from a starting to a final configuration, as we can see in Figure 1.1.

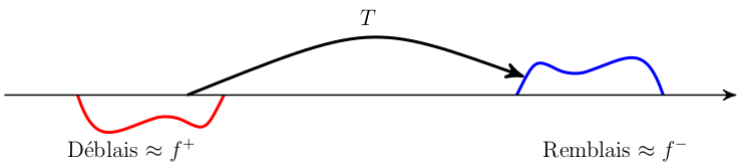

Figure 1.1: A schematic representation of Monge OTP formulation: find a map T moving the soil from one excavation f^+ to an embankment of equal volume f^- with minimal cost.

The mathematical formulation of the problem is the following: Let $\Omega \subset \mathbb{R}^d$ and consider two density functions f^+, f^-: $\Omega \to [0, \infty[$, with the additional condition $\int_\Omega f^+ = \int_\Omega f^-$. These density functions describes respectively the initial and the final configuration of the mass we want to optimally transport.

If we introduce a cost function $c : \Omega \times \Omega \to \mathbb{R}$, we would like to find the optimal solution T^* among all measurable maps $T : \Omega \to \Omega$, that is we are looking for:

$$T^* \in \inf_{T:\Omega\to\Omega} \left\{ \int_\Omega c(x, T(x)) df^+(x) \quad : T_\# f^+(A) = f^-(A),\ \forall A \in \Omega \text{ measurable} \right\}$$

where $T_\# f^+(A) := f^+(T^{-1}(A))$.
The original problem of Monge is a particular case of the following one, where the cost function $c(x, y) = |x - y|$.

Problem 1 (Monge Problem) Consider two complete and separable spaces X and Y. Given two non-negative measures f^+ and f^- on X and Y satisfying $f^+(X) = f^-(Y)$, a cost functional $c : X \times Y \to \mathbb{R}$, find $T^* \in \mathcal{T}(f^+, f^-) := \{\text{Measurable Maps } T : X \to Y \text{ s.t. } T_\# f^+ = f^-\}$, solving:

$$\min_{T\in\mathcal{T}(f^+,f^-)} I(T) := \int_X c(x, T(x)) df^+(x) \tag{1.1}$$

where $T_\#$ is defined as above.

In general Problem 1 is ill-posed and the optimal map may not even exist. For example, there are some problems when the measure f^+ is a Dirac measure and f^- is not. Moreover, a number of difficulties arise when trying to apply the direct method of the calculus of variation in order to find a optimal plan. Because of these mathematical difficulties, Leonid Kantorovich introduced a relaxed version of Problem 1.

1.2 Kantorovich Problem

This reformulation of Monge Problem was inspired by the following discrete Monge Problem:

Problem 2 (Discrete Monge Problem) Consider n points $(x_i)_{i=1,\dots,n} \in \mathbb{R}^d$ with associated masses $(f_i^+)_{i=1,\dots,n}$ and m points $(y_j)_{j=1,\dots,m} \in \mathbb{R}^d$ with associated masses $(f_j^-)_{j=1,\dots,m}$ with the requirement that $\sum_i^n f_i^+ = \sum_j^m f_j^-$. Given the real numbers $(c_{i,j})_{j=1,\dots,m}^{i=1,\dots,n}$ representing the cost of moving one unit of mass from x_i to y_j, we look for a solution $\gamma_{i,j}^*$ of the following minimization problem:

$$\min_{\gamma_{i,j}} \left\{ \sum_{i=1}^n \sum_{j=1}^m c_{i,j}\gamma_{i,j} : \sum_{i=1}^n \gamma_{i,j} = f_i^+,\ \sum_{j=1}^m \gamma_{i,j} = f_i^-,\ \gamma_{i,j} \geq 0 \right\} \tag{1.2}$$

The formulation of Problem 2 suggests us that we should search the solution of the OTP among the set of Transport Plans, instead of the transport maps.

Definition 1 *(Transport Plan):*

$$\Pi(f^+, f^-) := \{\gamma \in \mathcal{M}_+(X \times Y) \text{ s.t. } (\pi_x)_{\#\gamma} = f^+,\ (\pi_y)_{\#\gamma} = f^-\}$$

where π_x and π_y are projections maps $(x, y) \mapsto x$ and $(x, y) \mapsto y$ respectively.

The transport plan γ and the relative constraints are clearly the continuous version of $\gamma_{i,j}$ and its constraints of Equation (1.2). Its infinite dimensional version is known nowadays as *Kantorovich Primal Problem* and reads as follows:

Problem 3 *(Kantorovich Primal Problem). Given two non-negative finite measures f^+ and f^- on X and Y satisfying $f^+(X) = f^-(Y)$, and a given cost function $c : X \times Y \to \mathbb{R}^+$, find the optimal transport plan $\gamma^* \in \Pi(f^+, f^-)$ that solves:*

$$\min_{\gamma \in \Pi(f^+, f^-)} \mathcal{K}_c(\gamma) := \int_{X \times Y} c(x, y) d\gamma(x, y)$$

This problem admits also a Dual Problem:

Problem 4 *(Kantorovich Dual Problem). Given two non-negative finite measures f^+ and f^- on X and Y satisfying $f^+(X) = f^-(Y)$, and a given cost function $c : X \times Y \to \mathbb{R}^+$. Let $\mathcal{L}_c$ be the set:*

$$\mathcal{L}_c := \{(u, v) \in \mathcal{C}_b(X) \times \mathcal{C}_b(Y) \text{ s.t. } : u(x) + v(y) \leq c(x, y)\ \forall (x, y) \in X \times Y\}$$

Find $(u^*, v^*) \in \mathcal{L}_c$ solving the maximization problem:

$$\sup_{(u,v) \in \mathcal{L}_c} \mathcal{I}_{(f^+, f^-)}[u, v] := \int_X u(x) df^+(x) + \int_Y v(y) df^-(y) \tag{1.3}$$

In [12] we can see why Problem 3 is a weaker formulation than Problem 1. Moreover, denoting with $\mathcal{C}_b(X)$ the space of continuous and bounded functions on X, the following results hold:

Theorem 1 *For any $c : X \times Y \to \mathbb{R}$ lower semi-continuous, Problem 3 admits a solution $\gamma^* \in \Pi(f^+, f^-)$.*

Theorem 2 *(Kantorovich Duality):*
Given two non-negative finite measures f^+ and f^- on X and Y satisfying $f^+(X) = f^-(Y)$, and a given cost function $c : X \times Y \to \mathbb{R}$ lower semi-continuous, the following equality holds:

$$\min_{\gamma \in \Pi(f^+, f^-)} \mathcal{K}_c(\gamma) = \max_{(u,v) \in \mathcal{L}_c} \mathcal{I}_{(f^+, f^-)}[u, v]$$

Theorem 3 *(Duality Result of Linear Programming):*
Let $A \in \mathbb{R}^{m,n}$, $x, c \in \mathbb{R}^n$ and $y, b \in \mathbb{R}^m$, then the following equality holds:

$$\min_x\{c \cdot x \quad \text{s.t.} : \quad \mathrm{x} \geq 0 \quad \mathrm{Ax} = \mathrm{b}\} = \max_{\mathrm{y}}\{\mathrm{b} \cdot \mathrm{y}\ \mathrm{s.t.} : \mathrm{A^T y} \leq \mathrm{c}\} \tag{1.4}$$

Remark 1 *Problem 4 can be seen as the extension of the dual of Problem 1, that is:*

$$\max \sum_{i=1}^{n} u_i f_i^+ + \sum_{j=1}^{m} v_j f_j^-$$

where $u_i + v_j \leq c_{i,j}\ \forall i = 1, \ldots, n;\ j = 1, \ldots m$. Moreover, Theorem 2 can be viewed as the extension of Theorem 3.

1.3 Links between Monge and Kantorovich formulations

In the previous sections we introduced two different formulations for OTP. Now we'are looking for some conditions to ensure an equivalence between Monge and Kantorovich formulations. As in [12] we want to report a result that ensures uniqueness of an optimal transport plan that is a solution of Kantorovich Primal Problem (see Problem 3) and also the existence of an optimal transport map for Monge Problem (see Problem 1).

Proposition 1 *Consider a compact domain $\Omega \subset \mathbb{R}^d$, two balanced measures $f^+, f^- \in \mathcal{M}_+(\Omega)$, such that $\partial\Omega$ is f^+-negligible and f^+ is absolutely continuous with respect to Lebesgue measure. If the transport cost is of the form $c(x, y) = h(|x - y|)$, where h is a strictly-convex function, then there exist a unique transport plan $\gamma^* \in \Pi(f^+, f^-)$ of the form $\gamma^* = (Id, T^*)_{\#} f^+$, with $T^* \in \mathcal{T}(f^+, f^-)$. Moreover, there exist a Kantorovich potential u and T^* satisfies the following relation:*

$$T^*(x) = x - (\nabla h)^{-1}(\nabla(u^*(x)))$$

For further information about this result, see [24]. We can see immediately how Proposition 1 is fundamental for the so-called L^p-OTP in which the cost reads as $c(x, y) = |x - y|^p$, where $p > 1$.

1.4 L^1-OTP

In this section we summarize a number of results on the L^1-OTP, due to its rich mathematical theory. We are using the following restricted hypothesis:

$X = Y = \Omega$, where $\Omega \subset \mathbb{R}^d$ is an open, bounded, connected and convex domain with a smooth boundary. In all this section we are omitting all the proofs of the results shown (see [12] for further information about proofs and where to find them).

Theorem 4 *(Kantorovich-Rubinstein Theorem)*
Consider $\Omega \subset \mathbb{R}^d$ as above. Take two non-negative measures f^+ and f^- on Ω such that $df^+(\Omega) = df^-(\Omega)$. The Kantorovich Dual Problem in Equation (1.3) with cost function $c(x, y) = |x - y|$ can be rewritten as find $u \in Lip_1(\Omega)$ that solves:

$$\sup_{u \in Lip_1(\Omega)} \int_\Omega u \, df \tag{1.5}$$

where $f := f^+ - f^-$ and $Lip_1(\Omega)$ is the set of the Lipschitz continuous functions of Ω such that their Lipschitz constant is 1.

Problem 5 *(Beckmann Problem)*
Consider $\Omega \subset \mathbb{R}^d$ as above. Take two non-negative measures f^+ and f^- on Ω such that $df^+(\Omega) = df^-(\Omega)$. Let $f = f^+ - f^-$. Find $v^* \in [\mathcal{M}(\Omega)]^d$ solving

$$\inf_{v \in [\mathcal{M}(\Omega)]^d} \left\{ \int_\Omega |v| \, dx \ : \ \mathrm{div}(v) = f \right\} \tag{1.6}$$

The divergence constraint on v is in the sense of distributions:

$$\int_\Omega \nabla \varphi \cdot dv = - \int_\Omega \varphi df \quad \forall \varphi \in \mathcal{C}^1(\bar{\Omega})$$

Now we can enunciate the following Proposition that states an equivalence between the minimization Problem described in 5 and the Problem described by Equation (1.5).

Proposition 2 *Consider $\Omega \subset \mathbb{R}^d$ an open, bounded, connected and convex domain with smooth boundary. Take two non-negative measures f^+ and f^- on Ω such that $df^+(\Omega) = df^-(\Omega)$ and $f = f^+ - f^-$, then Problem 5 and Equation (1.5) are equivalent, which means:*

$$\sup_{u \in Lip_1(\Omega)} \int_\Omega u \, df = \inf_{v \in [\mathcal{M}(\Omega)]^d} \left\{ \int_\Omega |v| \, dx \ : \ \mathrm{div}(v) = f \right\}$$

Definition 2 *(Optimal Transport Density):*
Let Ω, f^+ and f^- as above. Given $\gamma^* \in \Pi(f^+, f^-)$ a minimizer for the Kantorovich Primal Problem (see Problem 3) with cost function $c(x, y) =$

$|x-y|$, the Optimal Transport Density $\mu^* \in \mathcal{M}_+(\Omega)$ associated to f^+, f^- is defined as:

$$\langle \mu^*, \varphi \rangle := \int_{\Omega\times\Omega} \int_0^1 \left|w'_{x,y}(t)\right| \varphi(w_{x,y}(t))\, dt\, d\gamma(x,y) \quad \forall \varphi \in \mathcal{C}(\Omega) \tag{1.7}$$

where $w_{x,y}(t) := (1-t)x + ty$

Theorem 5 *Let Ω, f, f^+ and f^- as above. If f^+ (or f^-) admits L^1-density with respect to the Lebesgue measure, then the OT density μ^* associated to f^+, f^- is uniquely defined and admits L^1-density with respect to the Lebesgue measure and we will indicate it with $\mu^*(f^+, f^-)$ (or with $\mu^*(f)$). Moreover, if f^+ and f^- admit L^p-densities for $1 \le p \le +\infty$, then the same holds for μ^*.*

Proposition 3 *Let Ω, f, f^+ and f^- as above. If f^+ and f^- admits L^p-density with $1 \le p \le +\infty$, then a solution v^* of Problem 5 is in $[L^p(\Omega)]^d$ and it can be written as*

$$v^* = -\mu^* \nabla u^* \tag{1.8}$$

where $\mu^* := \mu^*(f)$ and $u*$ is solution of the Dual Kantorovich Problem (see Problem 4).

Remark 2 *The previous Proposition gives us a way to find a solution of Beckmann Problem (Problem 5) when $\mathcal{M}(\Omega) = L^1(\Omega)$. Moreover, the solution v^* is a minimum.*

Now we can state the main result of this section about $L^1 - OTP$.

Proposition 4 *(Monge-Kantorovich Equations)*
Let Ω, f, f^+ and f^- as above. If f^+ (or f^-) admits L^1-density, then the OT-density $\mu^*(f)$ and the Kantorovich potential u^* solve the following equations:

$$-\operatorname{div}(\mu^* \nabla u^*) = f \qquad \text{in } \Omega \tag{1.9}$$

$$|\nabla u^*| \le 1 \qquad \text{in } \Omega \tag{1.10}$$

$$|\nabla u^*| = 1 \qquad \text{a.e. in } \mu^* > 0 \tag{1.11}$$

1.4.1 Monge-Kantorovich Equations applications to other problems

Here we look quickly at other ways to use MK Equations. The hypothesis on Ω, f^+, f^- and $f = f^+ - f^-$ are still valid.

Problem 6 *(Mass Optimization Problem) (see [7] for further details)*
Under the above hypothesis, find $v^* \in \mathcal{M}_+(\Omega)$ *that solves*

$$\min_{v \in \mathcal{M}_+(\Omega)} \{\mathcal{E}_f(v) \quad : \quad v(\Omega) = 1\}$$

where:

$$\mathcal{E}_f(v) := \sup_{\varphi \in \mathcal{C}^1(\Omega)} \Gamma_f(v, \varphi) \tag{1.12}$$

$$\Gamma_f(v, \varphi) := \int_\Omega (\varphi df - \frac{|\nabla \varphi^2|}{2} dv) \tag{1.13}$$

Proposition 5 *Given the OT density* $\mu^*(f)$*, a solution of Problem 6 is given by:*

$$v^* = \frac{\mu^*}{\int_\Omega d\mu^*}$$

The MK equations are linked to the ∞-Poisson Equation as the following Proposition states.

Proposition 6 *(∞-Poisson)*
Under the above hypothesis, if f^+ *and* f^- *admit Lipschitz continuous densities with respect to the Lebesgue measure, then the solution pair* (μ^*, u^*) *of* (1.9) *is the limit for* $p \to \infty$ *of* $(|\nabla u_p|^{p-2}, u_p)$ *in where* u_p *solves the p-Poisson equations:*

$$-\operatorname{div}(|\nabla u_p|^{p-2} \nabla u_p) = f$$

The limit for the first term must be understood in the sense of the weak topology on $L^\infty(\Omega)$

We can now introduce the first explicit solution of Monge Problem (see Problem 1) that can be found in [11].

Proposition 7 *(Solution of the Monge Problem)*
Consider Ω*,* f^+*,* f^- *and* f *as above. Assume that* f^+ *and* f^- *admit Lipschitz continuous densities with respect to the Lebesgue measure. Take* $x \in supp(f^+)$ *and consider the solution* $z(t, x)$ *of the following ODE:*

$$z'(t) = Z(t, z(t))$$

where $z(0) = x$ *and*

$$Z(t, z) := \frac{-\mu^*(z) \nabla u^*(z)}{(1-t) f^+(z) + t f^-(z)}$$

So the map $T^* : supp(f^+) \to supp(f^-)$ *such that* $x \mapsto z(1, x)$ *is the solution of the Monge Problem with cost equal to Euclidean distance.*

In [12] there is a generalized version of the L^1-OTP in which a geodetic distance is used instead of Euclidean distance. Moreover, there is also a figure (see page 22) that shows the links between all the formulations that have been written in the previous pages.

1.5 Branched Transport Problems

In the previous sections the total transport cost does not depend on the intermediate phases between the initial and the final configurations of the mass, but in many real-life problems we want to study transport mechanisms in which mass concentration is favored or penalized. Gilbert in [15] was the first one who gave a formulation of Branched Transport Problem (BTP) as a problem of finding the minimal cost of a communication network. This problem was extended in the following years even if it has the big issue of having a NP hard numerical solution, even in the discrete case. In all this section, we're using the same notation as [3].

1.5.1 The Gilbert-Steiner Problem

In most transportation networks, the aggregation of mass on common routes is often preferable to individual straight paths. The Steiner model consists in minimizing the total length of a network connecting a given set of points. This is not realistic because the fact that different paths could have different costs is not considered. Gilbert was the first one to propose a model which considers this fact in [15].

Definition 3 *(Gilbert Graph)*
The network is a graph such that each edge e is associated with a flow $\varphi(e)$. Let $f(\varphi)$ denote the cost per unit length of an edge with flow φ. It is assumed that $f(\varphi)$ satisfies the following properties:

1. *$f(\varphi)$ is subadditive, i.e., $f(\varphi_1) + f(\varphi_2) \geq f(\varphi_1 + \varphi_2)$*
2. *$f(\varphi)$ is increasing, i.e, $f(\varphi_1 + \varphi_2) \geq \max\{f(\varphi_1), f(\varphi_2)\}$*

Our task is to find the minimum cost of networks supporting a given set of flows between terminals.

Remark 3 *The subadditivity of $f(\varphi)$ translates the fact that it is more advantageous to transport flows together and it leads to delay bifurcations.*

Fluid mechanics gives us an example of this behavior, which is granted by Poiseuille's law, according to which the resistance of a tube increases when it gets thinner. The simplest model of this kind is to take $f(\varphi) = \varphi^\alpha$ where $0 < \alpha < 1$.
In [15], Gilbert considered atomic sources $\mu^+ = \sum_{i=1}^k a_i \delta_{x_i}$ and sinks $\mu^- = \sum_{j=1}^l b_j \delta_{y_j}$, where $\sum_i a_i = \sum_j b_j$ and $a_i, b_j > 0 \ \forall i = 1, \dots, k;\ j = 1, \dots, l$.

Definition 4 *(Transport Path)*
An admissible Transport path G is a weighted directed graph with straight edges $E(G)$ and a flow function $\varphi : E(G) \to (0, \infty)$ satisfying Kirchhoff's Law. G can be written as a vector measure

$$G = \sum_{e \in E(G)} \varphi(e) \mathcal{H}^1|_e \mathbf{e} \tag{1.14}$$

where $\mathbf{e}$ denotes the unit vector in the direction of e and $\mathcal{H}^1$ is the Hausdorff one-dimensional measure. We say that G irrigates (μ^+, μ^-) if its distributional derivative satisfies $\partial G = \mu^- - \mu^+$.
The Gilbert energy of G is defined by:

$$M^\alpha(G) = \sum_{e \in E(G)} \varphi(e)^\alpha \mathcal{H}^1(e) \tag{1.15}$$

Problem 7 *(Gilbert Problem)*
The Gilbert-Steiner Problem is the problem of minimizing $M^\alpha(G)$ among all infinite graphs irrigating (μ^+, μ^-), i.e. we want to find the Transport Path in $(G, \varphi) \in \mathcal{P}(\mu^+, \mu^-)$ that minimizes the Gilbert Energy.

We can see that this problem generalizes Monge-Kantorovich Problem ($\alpha \to 1$) and Steiner Problem ($\alpha = 0$). The intermediate case with $0 < \alpha < 1$ is the starting point of the so called Branched Transport Problem (BTP).
There was some extension to the continuous case of Problem 7. We briefly report here some of them.

Xia's Transport Paths

Definition 5 *(Xia's Transport path and its energy)*
Let μ^+ and μ^- be two positive Radon measures with equal mass in a compact convex set $X \subset \mathbb{R}^N$. A vector measure T on X with values in $\mathbb{R}^N$ is called a transport path from μ^+ to μ^- if there exist two sequences μ_i^-, μ_i^+ of finite atomic measures with equal mass and a sequence of finite graphs G_i irrigating

(μ_i^+, μ_i^-) such that $\mu_i^+ \to \mu^+$, $\mu_i^- \to \mu^-$ weakly as measures and $G_i \to T$ as vector measures. The energy of T is defined by:

$$M^\alpha(T) := \inf_A \liminf_{i\to\infty} M^\alpha(G_i) \tag{1.16}$$

where:

$$A := \{(\mu_i^+, \mu_i^-, G_i) \ : \ \textit{approximating sequences to } T\}$$

Later we're using also the following notation:

$$M^\alpha(\mu^+, \mu^-) := \inf\{M^\alpha(T) \ : \ \text{T is a transport path from } \mu^+ \text{ to } \mu^-\}$$

Xia showed the existence and the finiteness of the above infimum for any pair (μ^+, μ^-) when $\alpha \in (1 - \frac{1}{N}, 1]$ in [33].

Traffic Plans

Bernot, Caselles and Morel in [2] extended the previous formalism to the case where the source is any Radon Measure.

Definition 6 *Let K be the set of 1-Lipschitz maps $\gamma : \mathbb{R}^+ \to X$. We define a distance on K by:*

$$d(\gamma, \gamma') := \sup_{k\in\mathbb{N}^*} \frac{1}{k} \, ||\gamma - \gamma'||_{L^\infty([0,k])}$$

which corresponds to the metric d of uniform convergence on compact sets.

Lemma 1 *The metric space (K,d) is compact.*

(See [3] for a proof.)

Definition 7 *Let $\gamma \in K$. We define its stopping time as:*

$$T(\gamma) := \inf\{t \geq 0 \ : \ \gamma \textit{ constant on } [t, \infty)\}$$

and the length of $\gamma([0, T(\gamma)])$ by $L(\gamma)$.

Remark 4 *The following properties hold:*

1. *γ is 1-Lispchitz so $L(\gamma) \leq T(\gamma)$*
2. *The stopping time $T : K \to \mathbb{R}^+$ is lower semi-continuous and therefore measurable. (see [3] for a proof)*

So we can now introduce the definition of a Traffic Plan.

Definition 8 *(Traffic Plan)*
A traffic plan $\boldsymbol{P}$ *is a positive measure on* $(K, \mathcal{B})$ *such that* $\int_K T(\gamma) d\mathbf{P}(\gamma) < \infty$. *We denote by* $TP := TP(X)$ *the set of all traffic plans in* X *and by* $TP_C := TP_C(X)$ *the set of traffic plans* $\boldsymbol{P}$ *such that* $\int_K T(\gamma) d\mathbf{P}(\gamma) \leq C$

This model allows one to add *who goes where* constraints to the optimization problem (this is the starting point of the so-called "Mailing Problem").

Further Considerations

There were also other extensions to the continuous case of Problem 7. We can cite for example a Lagrangian formulation made by Maddalena and Solimini. The solutions of this models are called patterns. For further information see [20] or [3].
We would like to report some comments about these models. Firstly, there is a consistency problem: when the irrigated measures μ^+ and μ^- are finite atomic, do the minimizers for all continuous models coincide with the Gilbert minimizer? Moreover, if μ^+ and μ^- are two general positive measures with equal mass, are the Xia's minimizers also optimal traffic plans and conversely? Finally, when $\mu^+ = \delta_s$ is a single source, are optimal patterns and optimal traffic plans equivalent notions? The answer of all these questions are a consequence of a main structure property of optimal traffic plans.
In the next pages we discuss some further properties about Xia's formulation and traffic plans and some conditions for the equivalence of the continuous extensions of the discrete Gilbert-Steiner Problem by Xia and Maddalena and Solimini (see Problem 7).

1.5.2 Xia's Formulation

In this section we're following the summary on this problem that can be find in [12]. Xia's original idea in order to extend Problem 7 to the continuous case is to consider two sequence of atomic measures $\mu_n^{\pm} \to \mu^{\pm}$ and define the optimal Transport Path from μ^+ to μ^- as the limit of the optimal Transport Paths $(\mathcal{P}_n^*, q_n^*) \in \mathcal{P}(\mu_n^+, \mu_n^-)$.
Now we need to introduce the notion of 1-rectificable set in $\mathbb{R}^d$ without specifying too many technical details. A subset K of E is 1-rectificable if there exist a countable set of smooth (continuous and differentiable) maps $f : \mathbb{R} \to \mathbb{R}^d$ such that the $\mathcal{H}^1$ measure of $E \setminus K$ is zero. We can think of it as a countable union of Lipschitz curves that "fills" K. Now consider a triple made of a 1-rectificable set $K \subset \Omega$, a vector field $\tau : K \to S^{d-1}$ and a function

$\varphi : K \to \mathbb{R}^+$ integrable with respect the 1-dimensional Hausdorff measure $\mathcal{H}^1$. So we can define a vector measure $v = [K, \tau, \varphi] \in [\mathcal{M}(\Omega)]^d$ through the following equation:

$$\langle [K, \tau, \varphi], \zeta \rangle := \int_K \varphi(x)\tau(x) \cdot \zeta(x) d\mathcal{H}^1(x) \quad \zeta \in [\mathcal{C}(\Omega)]^d$$

We associate to a given path $(G, \varphi) \in \mathcal{P}(\mu^+, \mu^-)$ the vector measure $v_{G,\varphi}$ composed by the triple $[E, \tau_E, \varphi]$, where E is the union of the graph edges, τ_E is the vector measure with unit value defined by the edge direction and φ is the weight satisfying Kirchhoff's Law, which can be rewritten as $\operatorname{div}(v_{G,\varphi}) = \mu_n^+ - \mu_n^-.$, or, if we write it in the sense of distributions, we obtain:

$$\int_\Omega \nabla\phi \cdot dv_{G,\phi} = -\int_\Omega \phi(d\mu_n^+ - d\mu_n^-) \quad \forall \phi \in \mathcal{C}^1(\Omega)$$

then the Gilbert-Steiner energy in equation (1.15) becomes:

$$M^\alpha(G, \varphi) = \sum_{e \in E(G)} (\varphi(e))^\alpha \mathcal{H}^1(e) = \int_{E(G)} |\varphi(x)|^\alpha \, d\mathcal{H}^1(x)$$

We can now extend this definition to a general $v \in [\mathcal{M}(\Omega)]^d$ as follows:

$$M^\alpha(v) := \inf \left\{ \liminf_n M^\alpha(G_n, \varphi_n) : \begin{array}{c} v_{(G_n,\varphi_n)} \rightharpoonup v \\ \text{and} \\ \mu_n^+ - \mu_n^- \rightharpoonup \mu^+ - \mu^- \\ \text{and} \\ \operatorname{div}(v_{(G_n,\varphi_n)}) = \mu_n^+ - \mu_n^- \end{array} \right\} \quad (1.17)$$

This implies that:

$$M^\alpha(v) = \begin{cases} \int_{E(G)} |v|^\alpha \, d\mathcal{H}^1(x) & \text{if } v = [E, \tau, \varphi] \\ \\ +\infty & \text{otherwise} \end{cases}$$

So we can finally give the definition of the BTP for general $\mu^\pm \in \mathcal{M}_+(\Omega)$ as in [33].

Problem 8 *Find $v^* \in [\mathcal{M}(\Omega)]^d$ solving:*

$$\inf_{v \in [\mathcal{M}(\Omega)]^d} \{M^\alpha(v) \quad : \quad \operatorname{div}(v) = \mu^+ - \mu^-\}$$

In general, this problem may have no solution.

1.5.3 Bernot's Formulation

With the expression "Bernot's Formulation" we are referring to the results shown in [3]. The following results are based on the notion of Traffic Plan that we introduced before. We are going to show an application of this method to the Monge-Kantorovich Problem (see Problem 1 but we have to give some other definitions at first.

Definition 9 *Given a traffic plan P, consider the following maps:*

$$\begin{aligned} \pi_0 :& K \to X \\ & \gamma \mapsto \gamma(0) \end{aligned} \qquad \begin{aligned} \pi_\infty :& K \to X \\ & \gamma \mapsto \gamma(T(\gamma)) \end{aligned} \qquad \begin{aligned} \pi :& K \to X \\ & \gamma \mapsto (\gamma(0), \gamma(T(\gamma))) \end{aligned}$$

The positive measures on X and on $X \times X$ defined by:

$$\mu^+(\mathbf{P}) = \pi_{0\#}\mathbf{P} \quad \mu^-(\mathbf{P}) = \pi_{\infty\#}\mathbf{P} \quad \pi(\mathbf{P}) = \pi_\#\mathbf{P} = \pi_P$$

will be called respectively the irrigating measure, the irrigated measure and the transference plan of $\boldsymbol{P}$, where with the notation $f_\#A$ we mean the measure on X obtained by transporting the measure A on K by the map $f : X \to K$.

Definition 10 *(Pattern)*
A pattern is a traffic plan $\boldsymbol{P}$ such that $\mu^+(\mathbf{P}) = \delta_S$ for some source point $S \in X$. We denote by $TP(\nu^+, \nu^-)$ the set of traffic plans $\boldsymbol{P}$ such that $\mu^+(\mathbf{P}) = \nu^+$ and $\mu^-(\mathbf{P}) = \nu^-$.

It could be useful to introduce also the notion of parameterization of a traffic plan $\mathbf{P}$.

Proposition 8 *We can parameterize any traffic plan $\boldsymbol{P}$ by a measurable function $\chi : \Omega = [0, |\Omega|] \to K$ such that $P = \chi_\#\lambda$, where λ is the Lebesgue measure on Ω.*

We shall set $\chi(\omega, t) := \chi(\omega)(t)$. The function χ satisfies some regularity properties. We only state them. For a proof see chapter 3 of [3].

Proposition 9 *(Properties of χ)*

1. *Let $\chi : \Omega \to K$. The map $\chi : \Omega \times \mathbb{R}^+ \to X$ is measurable if and only if the map $\omega \in [0, |\Omega|] \mapsto \chi(\omega, \cdot) \in K$ is measurable.*
2. *Let $f : \Omega \times \mathbb{R}^+$ a function such that $\omega \mapsto f(\omega, t)$ is measurable for each $t \in \mathbb{R}^+$ and that $t \mapsto f(\omega, t)$ is continuous for every ω (f is called a Caratheodory function). Then f is measurable with respect to the σ-algebra generated by the product of Lebesgue measurable sets of Ω and Borelians of $\mathbb{R}^+$.*

After having shown some results about measurability, we can give some extensions of the previous definitions in the case of a parameterization.

Definition 11 *If $\chi : \Omega \times \mathbb{R}+ \to X$ is measurable, its stopping time is defined by:*

$$T(\omega) := T_\chi(\omega) := \inf\{t : \chi(\omega) \text{ is constant on } [t, \infty)\}$$

We also denote the length of the path $t \mapsto \chi(\omega, t)$ by $L(\omega)$.

Definition 12 *Let Ω be a measurable subset of $\mathbb{R}$ with finite measure. A parameterized traffic plan is a measurable map $\chi : \Omega \times \mathbb{R}^+ \to X$ such that $t \mapsto \chi(\omega, t)$ is 1-Lipschitz for all $\omega \in \Omega$ and $\int_\Omega T(\omega)d\omega < \infty$. Without risk of ambiguity we shall call fiber both a path $\chi(\omega, \cdot)$ and the range in $\mathbb{R}^N$ of $\chi(\omega, \cdot)$. $\mathbf{P}_\chi(E) = |\chi^{-1}(E)|$ is a traffic Plan for every Borel set $E \subset K$, where $|\chi| := |\Omega|$ is the total mass transported and $\mathbf{P}_\chi$ is the law of $\omega \to \chi(\omega) \in K$.*

Definition 13 *Let $\mathbf{P}_n$ be a sequence of traffic plans. We say that $\mathbf{P}_n$ converges to a traffic plan $\mathbf{P}$ if $\mathbf{P}_n \rightharpoonup \mathbf{P}$ or equivalently $\chi_n(\omega) \to \chi(\omega)$ in K for almost all $\omega \in \Omega$ as $n \to \infty$.*

Definition 14 *We call the cost of a traffic plan a functional*

$$I(\mathbf{P}) = \int_K c(\gamma(0), \gamma(T(\gamma))d\mathbf{P}(\gamma)$$

where $c(x, y)$ is a bounded non-negative lower semi-continuous function which represents "the cost for transporting a unit of mass from x to y".

Remark 5 *We can rewrite the Monge-Kantorovich Problem (see Problem 1) as it follows. Given two positive measures ν^+ and ν^- with equal mass, find a transference plan π that minimizes $\int_{X\times X} c(x, y)d\pi$. By definition of $\pi_\mathbf{P}$, we notice that $I(\mathbf{P}) = \int_{X\times X} c(x, y)d\pi_\mathbf{P}$. Moreover, it could be showed that any transference plan can be obtain as the transference plan of some traffic plan, so the problem of minimizing $I(\mathbf{P})$ under prescribed marginal measures $\mu^+(\mathbf{P}) = \nu^+$ and $\mu^-(\mathbf{P}) = \nu^-$ is equivalent to the Monge-Kantorovich transport Problem.*

Proposition 10 *The problem of minimizing $I(\mathbf{P})$, with $\mathbf{P} \in TP_C(\nu^+, \nu^-)$ admits a solution for C large enough.*

See Proposition 3.32 of [3] for a proof of this fact.

Definition 15 *Let $\alpha \in [0,1]$. The (Gilbert) energy of a traffic plan $\boldsymbol{P}$ parameterized by χ is the functional*

$$\mathcal{E}^\alpha(\boldsymbol{P}) = \int_\Omega \int_{\mathbb{R}^+} |\chi(\omega,t)|_\chi^{\alpha-1} |\dot{\chi}(\omega,t)| \, dt d\omega \tag{1.18}$$

Remark 6 *The energy of a traffic plan can also be written as*

$$\mathcal{E}^\alpha(\boldsymbol{P}) = \int_K \int_{\mathbb{R}^+} |\gamma(t)|_{\mathbf{P}}^{\alpha-1} |\dot{\gamma}(t)| \, dt d\mathbf{P}(\gamma)$$

Thus it is independent from the choice of the parameterization.

Proposition 11 *Consider two positive measures ν^+ and ν^- on X with equal mass. Assume that there exists at least one traffic plan connecting ν^+ to ν^- with finite energy. Then the problem of minimizing $\mathcal{E}^\alpha(\mathbf{P})$ in $TP(\nu^+,\nu^-)$ admits a solution. In the same way, the problem of minimizing $\mathcal{E}^\alpha(\mathbf{P})$ in $TP(\pi)$ admits a solution if there is at least one traffic plan $\boldsymbol{P}$ such that $\pi_{\mathbf{P}} = \pi$.*

Definition 16 *A traffic plan χ is said to be optimal for the irrigation problem, respectively optimal for the "who goes where" problem if it is of minimal cost in $TP(\mu^+(\chi), \mu^-(\chi))$, respectively in $TP(\pi_\chi)$.*

Definition 17 *(Generalized Gilbert Energy)*

$$E^\alpha(\mathbf{P}) := \int_{\mathbb{R}^N} |x|_{\mathbf{P}}^\alpha \, d\mathcal{H}^1(x)$$

We can see that Definition 17 generalizes the Gilbert Energy of 1.15 according to Bernot's notation.

Definition 18 *A traffic plan $\boldsymbol{P}$ is said to be loop-free if there is a parameterization χ of $\mathbf{P}$ so that for almost all $\omega \in [0,1]$, the element $\chi(\omega)$ of K is injective on $[0, T(\omega)]$.*

Proposition 12 *The minimum of $\mathcal{E}^\alpha$ on the set of traffic plans, if it exists, is attained at a loop-free traffic plan. Moreover $\inf \mathcal{E}^\alpha = \inf E^\alpha$, where both infima are taken indifferently over the set of all traffic plans or over the set of loop-free traffic plans.*

For a proof of this, see Proposition 4.9 of [3].
Now we enunciate an important result found by Bernot-Caselles-Morel without its proof (see [3]).

Proposition 13 *Consider two non negative measures μ^+ and μ^- on a domain X with the same mass M and consider $\alpha > 1 - 1/N$, where N is the dimension of the ambient space. Set:*

$$E^\alpha(\mu^+, \mu^-) := \min_{\chi \in TP(\mu^+, \mu^-)} E^\alpha(\chi)$$

the optimal cost to transport μ^+ to μ^-. Then $E^\alpha(\mu^+, \mu^-)$ is finite and can be bounded by:

$$E^\alpha(\mu^+, \mu^-) \leq C_{\alpha,N} M^\alpha diam(X)$$

where $C_{\alpha,N}$ and M are suitable constants and $diam(X)$ is the diameter of the domain X.

For a proof of this Proposition see Chapter 6 of [3]. Now we enunciate a structure theorem for optimal traffic plans. (see [3])

Theorem 6 *(Bernot-Caselles-Morel, 2009)*
Consider a traffic plan χ passing through the points x and y, then all the following properties hold:

1. *All fibers passing by x and y follow the same path.*
2. *If χ is an optimal traffic plan, then it has no circuits, i.e. χ is a tree.*
3. *If χ is an optimal traffic plan it can be monotonically approximated by finite irrigation graphs.*

All the proofs of Theorem 6 can be found in Chapter 7 of [3]. This is an important result because it suggests us to work with graphs in order to get an approximated solution of this BTP.
Now we are able to show the equivalences between Gilbert-Steiner Problem and optimal traffic plans formulation when μ^+ and μ^- are finite atomic. Moreover we can show also the equivalence between this formulation and Xia's one. All these equivalences are strong because not only the minimal energies are the same, but also the minimizing objects can be identified with each other even if they have a very different nature.

Proposition 14 *Let π be a transference plan between two finite atomic measures μ^+ and μ^-. An optimal traffic plan for the irrigating problem (see Definition 5) between μ^+ and μ^- is a finite graph made of segments with no circuits. Conversely, an optimal graph is an optimal traffic plan.*

A proof of this result can be found in Section 9.1 of [3]. We recall that we indicate the energy of Xia's problem with $M^\alpha(\mu^+, \mu^-)$.

Proposition 15 *Let (μ^+, μ^-) be two Radon measures of equal mass. Then:*

$$E^\alpha(\mu^+, \mu^-) = M^\alpha(\mu^+, \mu^-)$$

. Moreover, if these energies are finite, then the optima are the same.

This last proposition implies the equivalence between Xia's and Bernot's Problem and gives a link between the objects that minimize the two different energies. See Section 9.1 of [3] for a proof of this fact.

1.6 Conclusion

In this chapter we briefly introduced the OTP and enunciated some results about this mathematical theory at first. Then we analyzed various formulations of the BTP. We considered two of them mainly: Xia's formulation in order to link to [12] analysis on this problem and Bernot's one because we are using the results on branching angles found by Bernot-Caselles-Morel in [3] in the next section to compare them with the branching angles found by mathematical biologist who studied arterial networks in the last century. At the end of this chapter we showed the equivalence between these two formulations, so we can use all the theoretical results of both of them in order to study a biological application of the BTP.

Chapter 2

From Scaling Laws to Bifurcation Angles

A number of researcher studied the relation between the organismal basal metabolic rate B and the organismal mass M during the last two centuries. In this chapter we are going to review some of the relation between this empirical law, optimality principles and bifurcation angles in arterial system proposed in the biological literature.

2.1 Scaling Laws

In 1932 Max Kleiber ([19]) published his work in which he showed some empirical data in support of the existence of a power law between the basal metabolic rate and the mass of an organism. Early studies date back from the beginning of the 20th century, when modeling considerations where derived based on a rather small experimental basis. Later other authors showed the existence of an empirical scaling laws in accurate respiration trials of dogs and rabbits. We can find some of these first results in a paper of Harris and Benedict ([16]) published in 1919. The first fundamental work of our study was published in 1932 by Kleiber ([19]) and contained what we summarize as a conjecture.

Conjecture 1 *(Kleiber, 1932)*
In natural selection warm-blooded animals are the fittest in which the caloric requirements are in harmony with the hemodynamic possibilities of oxygen transport. This harmony seems to be established when the logarithm of the metabolism B is proportional to the logarithm of body weight M. Moreover, $\mathrm{B} = \mathrm{cM}^{\alpha}$*, where c is a suitable constant and* $\alpha \in [\frac{2}{3}, \frac{3}{4}]$.

Kleiber based his conjecture on the empirical data that he collected about animal and human metabolism. We can find all these results in [19]. In the last decades some authors cited Kleiber's paper to find an accurate scaling law. For instance, West, Brown and Enquist in 1997 ([30]) concluded the following:

Conjecture 2 *(West, Brown and Enquist, 1997)*
If the relations of Conjecture 1 reflect geometric constraints, then α should be a simple multiple of one-third. However, most biological phenomena scale as quarter rather than third powers of body mass.

They showed this conjecture in the following way: "For example, metabolic rates B of entire organisms scale as $M^{3/4}$; rates of cellular metabolism, heartbeat, and maximal population growth scale as $M^{-1/4}$. Sizes of biological structures scale similarly: for example, the cross-sectional areas of mammalian aortas and of tree trunks scale as $M^{3/4}$". [30] But no general theory explains the origin of these relations, so the authors supposed that a common mechanism underlies these laws.

Lemma 2 *(West, Brown and Enquist, 1997)*
A quantitative model that explains the origin and ubiquity of quarter-power scaling and predicts the essential features of transport systems, such as mammalian blood vessels and bronchial trees, is based on three unifying principles or assumptions:

1. *A space-filling fractal-like branching pattern is required in order for the network to supply the entire volume of the organism.*

2. *The final branch of the network is a size-invariant unit.*

3. *The energy required to distribute resources is minimized.*

The proof of this lemma is long and we do not report it, but it can be found in [30]. As Doods and others noticed in a paper in 2001 ([10]), this proof is based on the following four assumptions:

- Homoiotherms have evolved to minimize the rate at which they dissipate energy (a homoiotherm is an organism, such as a mammal or a bird, having a body temperature that is constant and largely independent of the temperature of its surroundings).

- The relevant energy dissipation arises from transport through nutrient-supplying networks.

- These networks are space-filling.
- All homoiotherms possess capillaries invariant in size.

Doods found some mathematical errors in the arguments used by West, Brown and Enquist, so the thesis of their Lemma can not be derived explicitly from their initial hypothesis. Nevertheless, their work is important in our context because there is a link between those Scaling Laws and the theory of arterial networks. Indeed, both these theories share the same hypothesis of the existence of an optimality principle. At first, the optimality principles provided the minimization of the energy lost during a laminar flow, but then other kinds of flows were studied, too.

2.2 Theoretical rules for bifurcations in Arterial Networks

One of the most obvious and classical invariant in a network having the previous characteristics is the distribution of branching angles, which is the invariant we are interested in this thesis. In this section we look for a historical and critical perspective at past attempts to characterize branching angles.
During the 19th century and the first two decades of the 20th century, a number of biologists dissected animals in order to understand the structure of circulatory system and to estimate the bifurcation angles in this network. For example, Murray mentioned the work of Hardy and Gardiner in a paper in 1926 (see [22]).
Now we are introducing the chronological evolution of this theory.

2.2.1 Murray's Law

We can suppose that Murray is the founder of a mathematical theory of branching angles in the circulatory system. Indeed, even if there are previous papers (we can mention for instance Hess's work of 1917 [17]), most of them are mathematically incorrect. Moreover, Murray's article of 1926 ([23]) received much attention in the literature, mostly because of his idea of minimizing the work made by the human body to spread blood through all its tissues.

Lemma 3 *(Murray, 1926)*
In a blood vessel of radius r, the flow of blood f is proportional to r^3. This relation is called "Murray's Law".

Proof[1]: We have to show that there exist a constant k depending only on the geometry of the blood vessel such that $f = kr^3$.
We can suppose that, if we consider an artery different from aorta, the blood satisfies a laminar flow in the vessel. Moreover, we can suppose also that arterial network has to satisfy a sort of "economy of circulation" that we wish. We work under two hypotheses:

1. Poisseuille's equation for the flow of liquids in cylindrical tubes follows

$$p = \frac{fl8\eta}{\pi r^4}$$

   where p is the difference in pressure between the two ends of the tube, f is the flow of liquid inside the tube, l is the length of the tube, r is its radius and η is the viscosity (if we multiply this quantity by f we obtain the first addend of the functional we would like to minimize).

2. There is a cost associated to the volume of blood involved in the flow give by $bl\pi r^2$, where b is the unit cost of blood that needs to be estimated during the process.

Under these hypotheses there are two further assumptions. Firstly, we have supposed that blood vessels can be approximated by a cylindrical tube in which there is a laminar flow of blood. Moreover, we have also supposed the existence of a maintenance cost for circulatory system.
If we multiply the first term by f and we sum the two addends, we obtain the following work E:

$$E = pf + bl\pi r^2 = \frac{f^2 l8\eta}{\pi r^4} + bl\pi r^2 \tag{2.1}$$

We want to minimize E, so, if we take the derivative of E with respect to r Equation (2.1) and we look for its zeros, we obtain:

$$\frac{\mathrm{dE}}{\mathrm{dr}} = -\frac{4f^2 l8\eta}{\pi r^5} + 2bl\pi r = 0 \tag{2.2}$$

This implies:

$$b = \frac{2f^2 8\eta}{n^2 r^6} \tag{2.3}$$

Now, if we recall the expression for pf, we can obtain an estimate for b, but we are not interested in this computation. Indeed, we rewrite Equation (2.3)

[1]We are using Murray's Proof, see [23]

in the following way:

$$f^2 = \frac{r^6 \pi^2 b}{16\eta} \tag{2.4}$$

If we take the square root of the expression for f given by Equation (2.4), we obtain the thesis:

$$f = kr^3 \tag{2.5}$$

where $k = \sqrt{\frac{\pi^2 b}{16\eta}}$ is a constant depending only on the geometry of the system and on the viscosity of the flow. □

Corollary 1 *If we indicate with r_0 the radius of the parent vessel and with r_1 and r_2 the radii of the children vessels, then the following equality hold:*

$$r_0^3 = r_1^3 + r_2^3$$

Proof: Since the flow in branches must equal the flow in the main steam, we have $f_0 = f_1 + f_2$. Moreover, we get $f_i = kr_i^3 \ \forall i = 0, 1, 2$ by Murray's Law. So the thesis follows immediately. □

2.2.2 Murray's Branching Angles

Starting from Lemma 3, Murray [22] tried to estimate the measure of branching angles in arterial network in another work of 1926. Before proceeding, we are recalling the principle of virtual work in classic mechanics, without its proof:

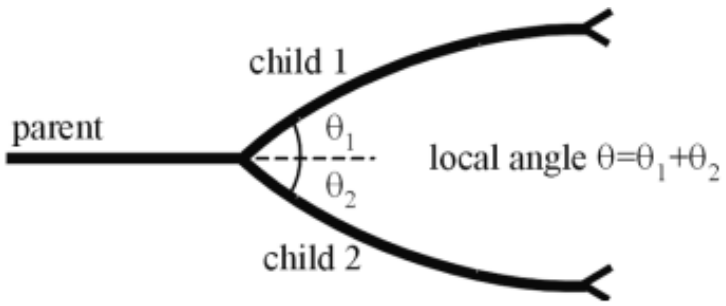

Figure 2.1: A schematic representation of a bifurcation angle from [8]

Proposition 16 ***(Principle of Virtual Work in Mechanics)*** *When conditions are such that the total work is a minimum, then a virtual change in the configuration of the system results in no change in the total work.*

Now we are able to prove another Lemma by Murray. In the following Lemma we are using notations by Changizi ([8]), as we did in Figure 2.1.

Lemma 4 *(Murray, 1926)*
If r_0 is the radius of the parent blood vessel, r_1 and r_2 are the radii of its children vessels and l_0, l_1 and l_2 are their respective lengths, then the system satisfies the following relation:

- $\cos(\theta_1) = \frac{r_0^4+r_1^4-r_2^4}{2r_0^2r_1^2}$
- $\cos(\theta_2) = \frac{r_0^4+r_2^4-r_1^4}{2r_0^2r_2^2}$
- $\cos(\theta) = \frac{r_0^4-r_1^4-r_2^4}{2r_1^2r_2^2}$

Remark 7 *Only two of these three relations are independent. Indeed, if we apply the addition formula:*

$$\cos(x+y) = \cos(x)\cos(y) - \sin(x)\sin(y)$$

we obtain that the third equation depends only on $\cos(x)$ *and* $\cos(y)$.

Proof[2]: Suppose that a minimum work condition is satisfied, as in Lemma 3, and suppose also a infinitesimal increment dl_0 to be added to l_0. Hence the "cost" of the section l_0 is now increased by the increment $dl_0r_0^2$, while the "costs" of branches are decreased by $\cos(\theta_1)dl_0r_1^2$ and $\cos(\theta_2)dl_0r_2^2$ respectively. Two similar constructions can be made, representing virtual increments added in turn to l_1 and l_2. By Proposition (16) we obtain one equation for each of the three configurations, as follows:

- $dl_0r_0^2 = \cos(\theta_1)dl_0r_1^2 + \cos(\theta_2)dl_0r_2^2$
- $dl_1r_1^2 = -\cos(\theta_1+\theta_2)dl_1r_2^2 + \cos(\theta_1)dl_1r_0^2$
- $dl_2r_2^2 = -\cos(\theta_1+\theta_2)dl_2r_1^2 + \cos(\theta_2)dl_2r_0^2$

If we divide them by dl_0, dl_1 and dl_2, respectively, and combine the three expressions, we obtain the thesis. □

Remark 8 *By Corollary 1 and Lemma 4 we can obtain these following equivalent formulations for the measure of the angles:*

- $\cos(\theta_1) = \frac{r_0^4+r_1^4-(r_0^3-r_1^3)^{4/3}}{2r_0^2r_1^2}$

[2]We are using Murray's Proof, see [22]

- $\cos(\theta_2) = \frac{r_0^4+r_2^4-(r_0^3-r_2^3)^{4/3}}{2r_0^2r_2^2}$
- $\cos(\theta_1+\theta_2) = \frac{(r_1^3-r_2^3)^{4/3}-r_1^4-r_2^4}{2r_1^2r_2^2}$

The proof is made of simple algebraic computations and we do not report it here.
Murray's ideas were highly appreciated by authors of the last century, but sometimes his results were not supported by empirical data. For this reason, some researcher started to change some of Murray's hypotheses in order to find more precise theoretical predictions on the measure of branching angles. They tried to do this in two different ways:

- They tried to consider different optimality principles.
- They tried to generalize Murray's work to the case of turbulent flows.

2.2.3 Zamir's Branching Angles

During the last quarter of the previous century Zamir proposed a more general method to compute bifurcation angles in arterial system (see [34]). He supposed that the geometry of an arterial junction is so designed as to minimize a functional H_h depending on some properties of blood flow and/or vessels in the junction. Moreover, he assumed that H_h is addictive, so that we can write $H_h = hl$, where l is the length of a vessel segment and h is the amount of value of H_h per unit length of that segment. Zamir analyzed different kind of bifurcations in his paper, but here we consider only a bifurcation similar to Figure 2.1. Let (x_0, y_0) the end point of the parent vessel and (x_1, y_1), (x_2, y_2) the final points of daughter vessels. Let also (x, y) the coordinates of the junction point. So, if $H_h = hl_0 + hl_1 + hl_2$, we can get the following:

$$H_h(x,y) = \sum_{i=0}^{2} h_i\sqrt{(x-x_i)^2+(y-y_i)^2} \tag{2.6}$$

Lemma 5 *(Zamir, 1976)*
If the functional H_h of Equation (2.6) *is minimized, the optimal values for branching angles are:*

- $\cos(\theta_1) = \frac{h_0^2+h_1^2-h_2^2}{2h_0h_1}$
- $\cos(\theta_2) = \frac{h_0^2+h_2^2-h_1^2}{2h_0h_2}$
- $\cos(\theta_1) = \frac{h_0^2-h_1^2-h_2^2}{2h_1h_2}$

Proof: If we rotate the system, we can always suppose that $y = y_0$. If we differentiate it with respect to x and y we obtain the Jacobian matrix J of H_h:

$$J = \begin{pmatrix} \frac{\partial H_h}{\partial x} \\ \\ \frac{\partial H_h}{\partial y} \end{pmatrix} = \begin{pmatrix} h_0 + \sum_{i=1}^{2} \frac{h_i(x-x_i)}{\sqrt{(x-x_i)^2+(y-y_i)^2}} \\ \\ \sum_{i=1}^{2} \frac{h_i(y-y_i)}{\sqrt{(x-x_i)^2+(y-y_i)^2}} \end{pmatrix} = \begin{pmatrix} h_0 - \sum_{i=1}^{2} h_i \cos(\theta_i) \\ \\ \sum_{i=1}^{2} (-1)^i h_i \sin(\theta_i) \end{pmatrix} \tag{2.7}$$

In a similar way, from (2.7) we can calculate the Hessian matrix A of H (we omit some computations):

$$A = \begin{pmatrix} \frac{\partial^2 H_h}{\partial x^2} & \frac{\partial^2 H_h}{\partial x \partial y} \\ \\ \frac{\partial^2 H_h}{\partial y \partial x} & \frac{\partial^2 H_h}{\partial y^2} \end{pmatrix} = \begin{pmatrix} \frac{h_0}{l_0} + \sum_{i=1}^{2} \frac{h_i}{l_i} \cos^2(\theta_i) & \sum_{i=1}^{2} (-1)^i \frac{h_i}{l_i} \cos(\theta_i) \sin(\theta_i) \\ \\ \sum_{i=1}^{2} (-1)^i \frac{h_i}{l_i} \cos(\theta_i) \sin(\theta_i) & \sum_{i=1}^{2} \frac{h_i}{l_i} \sin^2(\theta_i) \end{pmatrix} \tag{2.8}$$

The condition for H_h to be a minimum are:

$$J^{\mathrm{T}} = (0,0) \quad \det(A) > 0 \quad \frac{\partial^2 H_h}{\partial x^2} > 0$$

If we impose these conditions, we find the thesis after some other straightforward omitted computations. □

Later Zamir investigated on the optimality principles that could be used in place during the construction of an arterial system. He described four different principles. We recall that in biology the lumen is the inside space of a tubular structure, such as an artery.

1. An arterial junction is in an optimum state when the total lumen surface S of the arteries involved is at a minimum.

2. An arterial junction is in an optimum state when the total lumen volume V of the arteries involved is at a minimum.

3. An arterial junction is in an optimum state when the pumping power W required for pumping blood through that junction is at a minimum.

4. An arterial junction is in an optimum state when the total drag force T acting on its lumen walls is at a minimum.

In a fully developed Poiseuille flow through a vessel segment of radius r and length l, if f denotes the flow and η denotes the viscosity of blood, the four previous quantities that we would like to minimize can be written as:

1. $S = sl$, where $s = 2\pi r$.
2. $V = vl$, where $v = \pi r^2$.
3. $W = wl$, where $w = \frac{8\eta f^2}{\pi r^4}$.
4. $T = tl$, where $t = \frac{8\eta f}{r^2}$

In fact, the first two represent, respectively, the surface and the volume of a cylinder of radius r and height l, while the other two are the pumping power and the drag force that a flow f, having a viscosity η, acts on the walls of a cylinder with the same dimensions of the previous one.

Optimality Principle	$\cos(\theta_1)$	$\cos(\theta_2)$	$\cos(\theta)$
Min. Surface	$\frac{r_0^2+r_1^2-r_2^2}{2r_0r_1}$	$\frac{r_0^2+r_2^2-r_1^2}{2r_0r_2}$	$\frac{r_0^2-r_1^2-r_2^2}{2r_1r_2}$
Min. Volume	$\frac{r_0^4+r_1^4-r_2^4}{2r_0^2r_1^2}$	$\frac{r_0^4+r_2^4-r_1^4}{2r_0^2r_2^2}$	$\frac{r_0^4-r_1^4-r_2^4}{2r_1^2r_2^2}$
Min. Pumping Power	$\frac{(f_0^4/r_0^8)+(f_1^4/r_1^8)-(f_2^4/r_2^8)}{2(f_0^2f_1^2/r_0^4r_1^4)}$	$\frac{(f_0^4/r_0^8)+(f_2^4/r_2^8)-(f_1^4/r_1^8)}{2(f_0^2f_2^2/r_0^4r_2^4)}$	$\frac{(f_0^4/r_0^8)-(f_1^4/r_1^8)-(f_2^4/r_2^8)}{2(f_1^2f_2^2/r_1^4r_2^4)}$
Min. Drag Force	$\frac{(f_0^2/r_0^4)+(f_1^2/r_1^4)-(f_2^2/r_2^4)}{2(f_2f_1/r_0^2r_1^2)}$	$\frac{(f_0^2/r_0^4)+(f_2^2/r_2^4)-(f_1^2/r_1^4)}{2(f_0f_2/r_0^2r_2^2)}$	$\frac{(f_0^2/r_0^4)-(f_1^2/r_1^4)-(f_2^2/r_2^4)}{2(f_1f_2/r_1^2r_2^2)}$

Table 2.1: Zamir's branching angles for various optimality principles for a bifurcation similar to the one in Figure 2.1.

Corollary 2 *(Zamir, 1976)*
The angles written in Table 2.1 are the optimal values for branching angles when H is S, V, W, T, respectively. Moreover, if Murray's Law holds (see Lemma 3), then V is equivalent to W and S is equivalent to T.

Proof: If we apply Lemma 5 where H is substituted by the expressions for optimality principles written above, we find immediately the first thesis.
The second one follows immediately recalling that by Murray's Law: $f = kr^3$.
If we substitute this expression into the formulas for W and T we conclude.
□

2.2.4 Generalized Murray's Law and Angles

In the same years of Zamir, some other authors, such as Uylings (see [29]), Woldenberg and Horsfield (see [31] and [32]) tried to generalize Murray's Law removing the hypothesis of laminar fluid.

We do not report here their explicit computations. They used Murray's idea after having generalized the first term in the quantity E of Lemma 3. Their idea is to introduce an exponent $x \in [2.33, 3]$ that has to be estimated in order to satisfy the so called Generalized Murray's law:

$$f = kr^x \tag{2.9}$$

where k depends only on the geometry of the system (as in Lemma 3) and x depends only on the type of flow inside the blood vessel. If the flow is laminar, then $x = 3$ and we get Murray's Law; however, if the flow is turbulent, as it happens in the aorta for example, then the exponent x tends to 2.33. All the intermediate cases are described by an appropriate exponent x in that range.
Suppose now that, using the notation of Figure 2.1, $r_1 > r_2$ (this is always possible due to arbitrariness of daughter vessel names) and set $\alpha = r_2/r_1$, so $\alpha \in [0, 1]$.

Optimality Principle	$\cos(\theta_1)$	$\cos(\theta_2)$	$\cos(\theta)$
Min. Surface	$\frac{(1+\alpha^x)^{2/x}+1-\alpha^2}{2(1+\alpha^x)^{1/x}}$	$\frac{(1+\alpha^x)^{2/x}-1+\alpha^2}{2\alpha(1+\alpha^x)^{1/x}}$	$\frac{(1+\alpha^x)^{2/x}-1-\alpha^2}{2\alpha}$
Min. Volume	$\frac{(1+\alpha^x)^{4/x}+1-\alpha^4}{2(1+\alpha^x)^{2/x}}$	$\frac{(1+\alpha^x)^{4/x}-1+\alpha^4}{2\alpha(1+\alpha^x)^{2/x}}$	$\frac{(1+\alpha^x)^{4/x}-1-\alpha^4}{2\alpha^2}$
Min. Pumping Power	$\frac{(1+\alpha^x)^{4-8/x}+1-\alpha^{4x-8}}{2(1+\alpha^x)^{2-4/x}}$	$\frac{(1+\alpha^x)^{4-8/x}-1+\alpha^{4x-8}}{2\alpha^{2x-4}(1+\alpha^x)^{2-4/x}}$	$\frac{(1+\alpha^x)^{4-8/x}-1-\alpha^{4x-8}}{2\alpha^{2x-4}}$
Min. Drag Force	$\frac{(1+\alpha^x)^{2-4/x}+1-\alpha^{2x-4}}{2(1+\alpha^x)^{1-2/x}}$	$\frac{(1+\alpha^x)^{2-4/x}-1+\alpha^{2x-4}}{2\alpha^{x-2}(1+\alpha^x)^{1-2/x}}$	$\frac{(1+\alpha^x)^{2-4/x}-1-\alpha^{2x-4}}{2\alpha^{x-2}}$

Table 2.2: Woldenberg's branching angles for various optimality principles for a bifurcation similar to the one in Figure 2.1, depending only on $\alpha = r_2/r_1$ and x.

Corollary 3 *(Woldenberg and Horsfield, 1986)*
The angle written in Table 2.2 are the optimal values for branching angles when Generalized Murray's Law Equation (2.9) *holds.*

Proof: The thesis follows immediately proceeding as in the first step of Corollary 2 with Equation (2.9) instead of Murray's Law □

Remark 9 *The couples of optimality principles S,T and V,W are now equivalent if and only if $x = 3$, that is when Murray's law holds.*

2.3 Comparison between Theory and Empirical data

A number of authors in the last forty years tried to verify if Generalized Murray's Law (Equation (2.9)) holds for animal circulatory systems and to estimate the best fitting exponent x.
For example, Zamir studied the circulatory system of a rat in 1983 ([35]). He concluded that branching angles and branch diameters at bifurcation sites have to be governed by certain physiological rules that aim to increase the efficiency of arterial bifurcations as flow dividing units, although he didn't understand the case of branching angles completely. Zamir's results were similar to others of previous experiments on human and monkey cardiovascular systems. Branching diameters at bifurcation sites seem to follow a pattern that represent a compromise between the requirement for minimum lumen volume and minimum pumping power. Branching angles seems to satisfy the requirement for minimum drag force, too, but they follow this pattern with considerable scatter. Moreover, using the same notation of the previous sections, it seems that $\theta_1 < \theta_2$. Finally, the bifurcations seem to lie in a plane, that is the angle between the parent vessel and the children plane is very often smaller than 10 degrees.
In 2000 Changizi and Cherniak reported some empirical data for the best fitting exponent x (see [8]). They found that in larger arteries the flow is turbulent and x tends to 7/3, while in smaller arteries Murray's Law seems to hold. Moreover they constructed a series of minimal volume and minimal surface trees and they compared them with empirical data in order to find the best fitting exponent x. They noticed that the optimality principle of minimum volume seems to be more precise. They found that in general, x should be in a range between 2.60 and 2.70.
Another example of empirical is given by a paper of Taber and others in 2001 (see [25]). Here the authors studied the evolution of the cardiovascular system of a chicken embryo using a video recorder and a image analysis software. They already knew that in adult chickens generalized Murray's law holds for $x \simeq 3$ by previous papers. They found that this seems to hold also in the first days of life of a chicken embryo. This suggests that blood vessels flow the same basic morphogenetic rules throughout life.
Lastly, as Changizi and Cherniak said ([8]), "It is therefore implausible to suppose that arterial trees are actually global optimized [...]. Arterial geometry is not driven by a computationally sophisticated floorplan, and even if it were, the resources required to compute the optimal geometry for large portions of arterial networks are super-astronomical."

So we can conclude that Murray's generalized Law (Equation (2.9)) holds for different values of the best fitting exponent x depending on the species and on the type of blood flow.

2.4 More on bifurcation angles

The problem of bifurcation angles was treated also from a mathematical point of view within the theory of Gilbert-Steiner problem of optimal transportation networks. We're using some proofs of a work by Bernot-Caselles-Morel (see [3]) using the notation of Figure 2.2.

In all this section we will suppose the following hypothesis: let A_1, A_2, A_3

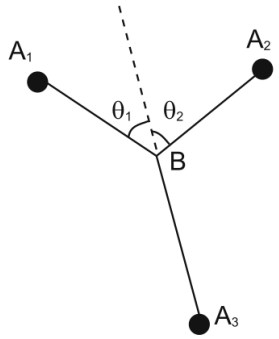

Figure 2.2: A schematic representation of a bifurcation angle by [3]

be three distinct point in $\mathbb{R}^N$, $\mu^- = m_1\delta_{A_1} + m_2\delta_{A_2}$ and $\mu^+ = m_3\delta_{A_3}$, three Dirac masses, with $m_3 = m_1 + m_2$ and $m_1, m_2 > 0$.
Firstly, we introduce the following Lemma without reporting its proof.

Lemma 6 *(Bernot, Caselles, Morel, 2009)*
In the case A_1, A_2, A_3 are aligned, an optimal traffic plan from μ^+ to μ^- has its support in the minimal segment containing A_1, A_2, A_3. If A_1, A_2, A_3 are not aligned, an optimal traffic plan has its support in the triangle A_1, A_2, A_3. In addition, it is a graph with two or three edges.

We can find the proof of Lemma 6 in chapter 12 of [3]. Now we are going to show the following Lemma about branching angles:

Lemma 7 *(Bernot, Caselles, Morel, 2009)*
Let $\boldsymbol{P}$ be an optimal traffic plan from μ^+ to μ^- made of three edges. With the notation of Figure 2.2, letting $\theta = \theta_1 + \theta_2$, the bifurcation point B has to

satisfy the following angle constraints:

$$\cos(\theta_1) = \frac{k_1^{2a} + 1 - k_2^{2a}}{2k_1^a} \tag{2.10}$$

$$\cos(\theta_2) = \frac{k_2^{2a} + 1 - k_1^{2a}}{2k_2^a} \tag{2.11}$$

$$\cos(\theta) = \frac{1 - k_2^{2a} - k_1^{2a}}{2k_1^a k_2^a} \tag{2.12}$$

where $k_1 = \frac{m_1}{m_1+m_2}$ *and* $k_2 = \frac{m_2}{m_1+m_2}$.

Proof: Because of Lemma 6, it is equivalent to consider the two dimensional situation, indeed this Lemma tells us that $\mathbf{P}$ has to be a segment or a triangle. Let us consider the graph $G(B)$ made of oriented weighed edges (A_1B, m_1), $(A_2B,_2)$ and (BA_3, m_3), with $B \in \mathbb{R}^2 \setminus \{A_1, A_2, A_3\}$. The cost of this graph is:

$$E^a(G(B)) = m_1^a \left|A_1B\right| + m_2^a \left|A_2B\right| + m_3^a \left|BA_3\right|$$

We can note that this function of B is differentiable on $\mathbb{R}^2 \setminus \{A_1, A_2, A_3\}$. Thus, if $G(B)$ is an optimal traffic plan with $B \notin \{A_1, A_2, A_3\}$, the first derivative of $E^a(G(B))$ has to cancel.
For $B \notin \{A_1, A_2, A_3\}$, let us denote by $\mathbf{n_i} = \frac{\mathbf{A_iB}}{||\mathbf{A_iB}||}$ the unit vector from A_i to B for $i = 1, 2, 3$. Since:

$$||\mathbf{A_iB} + \mathbf{v}|| = ||\mathbf{A_iB}|| + \mathbf{v} \cdot \mathbf{n_i} + o(||\mathbf{v}||),$$

the necessary condition given by the cancellation of the derivative of the cost function yields the balance equation:

$$m_1^a \mathbf{n_1} + m_2^a \mathbf{n_2} + m_3^a \mathbf{n_3} = 0 \tag{2.13}$$

Let θ_i be the angle between $\mathbf{n_i}$ and $-\mathbf{n_3}$ for $i = 1, 2$ and $k_1 = \frac{m_1}{m_1+m_2}$, $k_2 = \frac{m_2}{m_1+m_2}$. Multiplying the previous balance equation (2.13) by $\mathbf{n_i}$ for $i = 1, 2, 3$, we obtain the following equalities:

$$k_1^a + k_2^a \mathbf{n_1 n_2} = \cos(\theta_1) \tag{2.14}$$

$$k_1^a \mathbf{n_1 n_2} + k_2^a = \cos(\theta_2) \tag{2.15}$$

$$k_1^a \cos(\theta_1) + k_2^a \cos(\theta_2) = 1 \tag{2.16}$$

so that the angles have to satisfy (2.10), (2.11) and (2.12) respectively, indeed, if we recall that $\mathbf{n_1 n_2} = \cos(\theta)$, we can find (2.12) substituting (2.14) and (2.15) into (2.16). Now, substituting (2.12) into (2.14) and (2.15) we obtain (2.10) and (2.11) respectively. □

Lemma 7 is important to show the equivalence between this mathematical measure of branching angles and the ones in Table 2.2.

Corollary 4 *If $m_1 = r_1$ and $m_2 = r_2$, the bifurcation angles of Lemma 7 are equivalent to:*

1. *the Minimum Volume angles of Table 2.2 when $a = \frac{2}{x}$.*
2. *the Minimum Surface angles of Table 2.2 when $a = \frac{1}{x}$.*
3. *the Minimum Pumping Power angles of Table 2.2 when $a = \frac{2x-4}{x}$.*
4. *the Minimum Drag Force angles of Table 2.2 when $a = \frac{x-2}{x}$.*

Proof: The proof follows immediately recalling that $\alpha = r_2/r_1$ in Table 2.2 and that $k_1 = \frac{m_1}{m_1+m_2}$, $k_2 = \frac{m_2}{m_1+m_2}$ in Lemma 7. We are showing only the equivalence of $\cos(\theta)$ for the minimum surface angle.

$$
\begin{aligned}
\cos(\theta) &= \frac{1 - k_2^{2a} - k_1^{2a}}{2k_1^a k_2^a} && \text{(Lemma 7 angle)} \\
&= \frac{1 - (\frac{r_2^x}{r_1^x + r_2^x})^{2/x} - (\frac{r_2^x}{r_1^x + r_2^x})^{2/x}}{2\,(\frac{r_1^x}{r_1^x + r_2^x}\,\frac{r_2^x}{r_1^x + r_2^x})^{1/x}} && \text{(Hypotesis on } a \text{ and } k_i\text{)} \\
&= \frac{(r_1^x + r_2^x)^{2/x} - r_2^2 - r_1^2}{2 r_1 r_2} && \text{(L. C. D. on the numerator)} \\
&= \frac{(\frac{r_1^x + r_2^x}{r_1^x})^{2/x} - (\frac{r_2}{r_1})^2 - 1}{2\,\frac{r_2}{r_1}} && \text{(Divide both members by } r_1^2\text{)} \\
&= \frac{(\alpha^x + 1)^{2/x} - 1 - \alpha^2}{2\,\alpha} && \text{(Definition of } \alpha \rightarrow \text{ Table 2.2 angle)}
\end{aligned}
$$

The other proofs are similar, so we omit them. □

Corollary 4 gives us a link between the cost function of a Gilbert-Steiner problem of optimal transportation networks and the optimality principles studied by a number of authors in the last century in order to study arterial networks discussed previously.

2.5 Further Considerations

We have already seen the development of the theory of branching angles during the 20th century. There are also some more modern applications of this discipline. For example in 1999 Kitaoka and Others ([18]) managed to recreate a 3-D model of the human airway tree. Their computational algorithm had to follow nine empirical laws, some of them based directly on

Murray papers. The final result was a great approximation of the real human airway tree and has been very useful in order to study the evolution of pulmonary diseases. Indeed, in the last years a lot of authors applied some models based on Murray's idea about the approximation of blood flow. These models increased a lot the accuracy on detecting pulmonary diseases. Another application of Murray's ideas was for example the research for a cardiac computed tomography (see [26]).
So we can see that this arguments are largely used in modern medicine together with computer simulations of models.

Chapter 3

Dynamic Monge-Kantorovich and the numerical formulation of the BTP problem

We can divide the numerical problem of this thesis in three different parts. Firstly, we work as in [12] in order to obtain a numerical solution of BTP problem for our initial conditions and domain via the Dynamic Monge Kantorovich (DMK) formulation proposed in [12]. Then, we use other codes to transform this solution into a graph structure. Finally, we simplify this graph and we study the branching angles of the simplified graph.
In this chapter we are going to analyze the analytical and numerical theory behind the DMK problem.

3.1 Dynamic Monge-Kantorovich

In this section we are going to show the main results found in [12] that link dynamic Monge-Kantorovich Problem (see Problem 1) to a system of PDE's. There is no complete proof of this link, but there are some theoretical and numerical indications that support their thesis. They started their work analyzing the behavior of *Physarum Polycephalum* (PP), a mold that is able to find the most efficient network path between food sources in a maze. The PP in the channels of the maze is schematized as an undirected planar graph $G = (V, E)$, with positive edge length $\{L_e\}_{e \in E}$ and two nodes indices $(v = 1, n)$ where two unitary food sources are located. We associate a "conductivity" function D_e and a "potential" (or "pressure") function p_v to each edge and node respectively.

Problem 9 *Consider $e = (u, v)$ the edge of G connecting vertices u and v, $\sigma(v)$ the set of edges having the vertex v in common (this set is called also the "star" of v) and a non-decreasing function $g : \mathbb{R}^+ \to \mathbb{R}^+$ such that $g(0) = 0$. The problem is to find the optimal distribution (D_e, p_v) that satisfies:*

$$\sum_{e\in\sigma(v)} Q_e(t) = f_v = \begin{cases} +1 & v = 1 \\ -1 & v = n \\ +0 & v \neq 1, n \end{cases} \qquad \forall v \in V \quad (\text{"Kirchhoff-Law"}) \tag{3.1}$$

$$Q_e(t) = D_e(t)\frac{(p_u(t) - p_v(t))}{L_e} \qquad \forall e \in E \quad (\text{"Fick-Poiseuille"}) \tag{3.2}$$

$$D'_e(t) = g(|Q_e(t)|) - D_e(t) \qquad \forall e \in E \quad (D_e \text{ dynamics}) \tag{3.3}$$

$$D_e(0) = \hat{D}_e(0) > 0 \qquad \forall e \in E \quad (\text{initial data}) \tag{3.4}$$

In [6] and in [27] the case $g(x) = x$ was studied. The authors showed that the conductivity D_e tends to have a local support on the edges of the shortest path between the two external sources. Later it has been showed that D_e converges to the shortest path for a general planar graph G. Moreover, this model is equivalent to an optimal transport problem on the graph G if we consider a balanced forcing term f such that:

$$\sum_{v\in V} f_v = 0$$

This problem can be rewritten as finding $Q = \{Q_e\}_{e\in E}$ such that:

$$\min_{Q\in\{Q_e\}_{e\in E}} \sum_{e\in E} Q_e L_e \quad \text{s.t.:} \quad \sum_{e\in\sigma(v)} Q_e = f_e \quad \forall v \in V$$

3.1.1 Dynamic Monge-Kantorovich Model

Now we are generalizing the previous model by removing the graph structure and defining a new problem on an open bounded domain $\Omega \subset \mathbb{R}^n$ and restricting only to the case in which $g(x) = x$. The following Problem is related to Proposition 4.

Problem 10 *(Dynamic Monge-Kantorovich (DMK) Problem)*
Given a forcing function $f : \Omega \to \mathbb{R}$, a continuous analogue of the function f of Problem 9, DMK Problem is to find a pair of functions $(\mu, u) : [0, \infty] \times \Omega \to \mathbb{R}^+ \times \mathbb{R}^d$ that satisfies the following equations, complemented by zero Neumann

boundary conditions:

$$-\operatorname{div}(\mu(t,x)\nabla u(t,x)) = f(x) \tag{3.5}$$
$$\partial_t \mu(t,x) = \mu(t,x)\,|\nabla u(t,x)| - \mu(t,x) \tag{3.6}$$
$$\mu(0,x) = \mu_0(x) > 0 \tag{3.7}$$

where $\partial_t \mu$ and $\nabla = \nabla_x$ indicates partial differentiation with respect to time and spacial gradient, respectively.

Remark 10 *The previous generalization is justified by comparing the equations of Problem 9 with the ones of Problem 10. In fact, Equation* (3.5) *gives the spatial balance of a continuous Fick-Poiseuille flux $q = -\mu\nabla u$ with potential u (it generalizes the first two equations of Problem 9). Moreover, Equation* (3.6) *and* (3.7) *are the analogue in the continuous setting of the discrete dynamics described by the last two equations of Problem 9.*

In [14] the authors conjecture that the system of equations described in Problem 10 converges to an equilibrium state as $t \to +\infty$.

Remark 11 *Formally, if the system reaches an equilibrium state, then $\partial_t \mu$ has to vanish, so Equation* (3.6) *becomes the constraint stating that the norm of the gradient of u must be unitary, where μ is strictly greater than zero.*

The previous remark is crucial for the following

Conjecture 3 *The solution pair $(\mu(t,x), u(t,x))$ of Problem 10 with $f = f^+ - f^-$ converges to the pair (μ^*, u^*), where $\mu^* = \mu^*(f^+, f^-)$ is the OT density and u^* is a Kantorovich potential solution of the L^1-OTP (see Proposition 4).*

The same authors proved the following theorem in [13] in which they investigate about the kind of solution we expect to find for the system of equations of Problem 10. The boundlessness of ∇u does not let us to obtain a solution defined globally in time, but only on a neighborhood of the initial time.

Theorem 7 *Given Ω an open, bounded, convex and connected domain in $\mathbb{R}^d$ with smooth boundary, $f \in L^\infty(\Omega)$ with zero mean and $\mu_0 \in \mathcal{C}^\delta(\Omega)$ with $\mu_0 > 0$ and $0 < \delta < 1$, there exists $\tau_0 > 0$, depending on f and μ_0 such that the system (S) admits a unique solution pair*

$$(\mu, u) \in \mathcal{C}^1([0, \tau_0[, \mathcal{C}^\delta(\Omega)) \times \mathcal{C}^1([0, \tau_0[, \mathcal{C}^{1,\delta}(\Omega))$$

where:

$$(S) = \begin{cases} \int_\Omega \mu(t,x)\nabla u(t,x)\nabla\varphi(x)dx = \int_\Omega f(x)\varphi(x)dx \quad \forall\varphi \in \mathcal{H}^1(\Omega) \\ \partial_t\mu(t,x) = \mu(t,x)\left|\nabla u(t,x)\right| - \mu(t,x) \\ \mu(0,x) = \mu_0(x) > 0 \\ \int_\Omega u(t,x)dx = 0 \end{cases}$$

3.1.2 Lyapunov-Candidate functional

The previous result is only local in time, so it does not allow us to pass to the limit with $t \to \infty$ in (S), but we can identify a Lyapunov-candidate functional, i.e. a function that decreases along the $\mu(t)$-trajectories, as in [14]. It is defined for general $\mu \in L^1(\Omega)$ and it's given by:

$$\mathcal{L}(\mu) := \mathcal{E}_f(\mu) + \mathcal{M}(\mu) \tag{3.8}$$

where

$$\mathcal{E}_f(\mu) := \sup_{\varphi\in\mathcal{C}^1(\bar{\Omega})} \int_\Omega (f\varphi - \mu\frac{|\nabla\varphi|^2}{2})dx \qquad \mathcal{M}(\mu) := \frac{1}{2}\int_\Omega \mu dx \tag{3.9}$$

Remark 12 *$\mathcal{E}_f(\mu)$ has already been defined in the Mass Optimization Problem (see Problem 6) for a general $\mu \in \mathcal{M}_+(\Omega)$.*

Now we are going to enunciate some properties about this Lyapunov-candidate functional. See [12] for their proof.
If we restrict $f \in \mathcal{F}$ and $\mu \in \mathcal{D}$, then the functional can be rewritten as:

$$\mathcal{L}(\mu) := \frac{1}{2}\int_\Omega \mu\left|\nabla u(\mu)\right|^2 dx + \frac{1}{2}\int_\Omega \mu dx \tag{3.10}$$

Proposition 17 *The functional $\mathcal{L} : \mathcal{D} \to \mathbb{R}^+$ defined in Equation (3.10) is strictly decreasing in time along the solution $\mu(t)$ of the equations of Theorem 7 for $t \in [0, \tau(\mu_0)[$ and its time derivative is given by:*

$$\frac{d\mathcal{L}(\mu(t))}{dt} = -\frac{1}{2}\int_\Omega \mu(t)(|\nabla u(t)| - 1)^2(|\nabla u(t)| + 1)dx$$

We can see immediately that the time derivative of $\mathcal{L}$ along $\mu(t)$-trajectories is equal to zero only if $|\nabla u(t)| = 1$ on the support of $\mu(t)$. This gives us only one of the constraints of MK equations in this case too, without imposing the bound on the norm of the gradient in the whole domain.
The previous Proposition suggests us to investigate about a minimum of $\mathcal{L}$, since it's time decreasing. This fact let us to show the equivalence between the minimization of $\mathcal{L}(\mu)$ and the Beckmann Problem (see Problem 5), which is equivalent to solving the MK equations.

Proposition 18 *Given Ω an open, bounded, convex and connected domain in $\mathbb{R}^d$ with smoothing boundary and $f \in L^1(\Omega)$ with zero mean, then Beckmann Problem and the minimization of $\mathcal{L}$ are equivalent, which means:*

$$\min_{v \in [L^1(\Omega)]^d} \left\{ \int_\Omega |v| \, dx \ : \ \mathrm{div}(v) = f \right\} = \min_{\mu \in L^1_+(\Omega)} \mathcal{L}(\mu) \tag{3.11}$$

where $L^1_+(\Omega)$ is the space of non-negative function in $L^1(\Omega)$. Moreover, the OT density $\mu^*(f)$ is a point of minimum for $\mathcal{L}$.

The proof of this Proposition can be found in [12], where a duality result is used. We can see that Equation (3.11) provides further support to Conjecture 3.
This particular Lyapunov-candidate functional can be derived both from Mass Optimization Problem (see Problem 6) and Kantorovich Dual Problem (see Problem 4) as the author of [12] showed.

3.2 Numerical solution of MK equations using DMK

In this section we're describing the methods used in [12] to get a numerical solution of MK equations. See this work for further details.

3.2.1 Numerical discretization

Projection Spaces

The approach used to find a solution of the system of equation of Theorem 7 is based on the method of lines.
Spatial discretization is achieved by projecting the weak formulation of the system of equations onto a pair of finite dimensional spaces $(\mathcal{V}_h, \mathcal{W}_h)$. Consider a regular triangulation $\mathcal{T}_h$ of the polygonal domain Ω, characterized

by n nodes and m triangles and by the characteristic length of elements h. We also denote with $\mathcal{P}_0(\mathcal{T}_h(\Omega)) = \text{span}\{\psi_1(x), \dots, \psi_M(x)\}$ and $\mathcal{P}_1(\mathcal{T}_h(\Omega)) = \text{span}\{\varphi_1(x), \dots, \varphi_N(x)\}$ the spaces of element-wise constant functions and continuous and linear Lagrangian basis function, respectively, both defined on $\mathcal{T}_h(\Omega)$. We define $\mathcal{T}_{h/2}(\Omega)$ as the triangulation obtained refining each triangle $T_k \in \mathcal{T}_h(\Omega)$ (i.e. each triangle T_k is divided in 2^d sub-triangles having the gravity centers of the 2^{d-1}-faces contained in T_k as nodes). The choice for the space $\mathcal{V}_h$ is $\mathcal{V}_h = \mathcal{P}_{1,h} = \mathcal{P}_1(\mathcal{T}_h(\Omega))$. Two different choices of spaces are made for the projection of the dynamic equation of Theorem 7 by using $\mathcal{W}_h = \mathcal{P}_{0,h/2}$ or $\mathcal{W}_h = \mathcal{P}_{0,h} = \mathcal{P}_0(\mathcal{T}_h(\Omega))$.

Spatial Discretization

If we indicate with N and M the dimensions of $\mathcal{V}_h$ and $\mathcal{W}_h$, respectively, the discrete potential $u_h(t,x)$ and the diffusion coefficient $\mu_h(t,x)$ can be rewritten as:

$$u_h(t,x) = \sum_{i=1}^{N} u_i(t)\varphi_i(x) \quad \varphi_i \in \mathcal{V}_h \qquad \mu_h(t,x) = \sum_{k=1}^{M} \mu_k(t)\psi_k(x) \quad \psi_k \in \mathcal{W}_h$$

The previous finite elements discretization yields the following:

Problem 11 *Find the pair $(u_h(t,\cdot), \mu_h(t,\cdot)) \in \mathcal{V}_h \times \mathcal{W}_h$ such that solves the following system of equations for $t \geq 0$ with the zero-mean constraint $\int_\Omega u_h(x)dx = 0$:*

$$a_{\mu_h}(u_h, \varphi_j) = \int_\Omega \mu_h \nabla u_h \cdot \nabla \varphi_j dx = (f, \varphi_j) = \int_\Omega f\varphi_j dx \qquad j = 1, \dots, N \tag{3.12}$$

$$\int_\Omega \partial_t \mu_h \psi_l dx = \int_\Omega (|\mu_h \nabla u_h| - \mu_h)\psi_l dx \qquad l = 1, \dots, M \tag{3.13}$$

$$\int_\Omega \mu_h(0,\cdot)\psi_l dx = \int_\Omega \mu_0 \psi_l dx \qquad l = 1, \dots, M \tag{3.14}$$

We can rewrite Problem 11 in matrix form, indicating with $\mathbf{u}(t) = \{u_i(t)\}$ and $\boldsymbol{\mu}(t) = \{\mu_j(t)\}$, where $i = 1, \dots, N$ and $j = 1, \dots, M$, the vectors that describe the time evolution of the projected system. So we can write the

following index-1 nonlinear system of differential algebraic equations (DAE):

$$\mathbf{A}[\boldsymbol{\mu}(\boldsymbol{t})]\mathbf{u}(t) = \mathbf{b} \tag{3.15}$$

$$\mathbf{M}\frac{d}{dt}\boldsymbol{\mu}(t) = \mathbf{B}(\mathbf{u}(t))\boldsymbol{\mu}(t) \tag{3.16}$$

$$\mathbf{M}\boldsymbol{\mu}(0) = \boldsymbol{\mu}_0 \tag{3.17}$$

where the $N \times N$ stiffness matrix $\mathbf{A}$ is given by:

$$A_{i,j}[\boldsymbol{\mu}(t)] = \sum_{k=1}^{M} \mu_k(t) \int_\Omega \psi_k \nabla\varphi_i \cdot \nabla\varphi_j dx$$

and the N components of the source vector $\mathbf{b}$ are:

$$b_i = \int_\Omega f\varphi dx$$

We can remove the singularity caused by the homogeneous Neumann boundary conditions by forcing the solution $\mathbf{u}$ to remain orthogonal to the vector:

$$a_i = \int_\Omega \varphi_i dx$$

The $M \times M$ mass matrix $\mathbf{M}$ and the $M \times M$ matrix $\mathbf{B}$ are defined as:

$$M_{k,l} = \int_\Omega \psi_k\psi_l dx \qquad B_{k,l}[\mathbf{u}(t)] = \int_\Omega \left(\left| \sum_{i=1}^{N} u_i(t)\nabla\varphi_i \right| - 1 \right) \psi_k\psi_l dx$$

Then the M-dimensional vector μ_0 contains the projected initial condition:

$$\mu_{0,l} = \int_\Omega \mu_0\psi_l dx$$

We can observe that, if we consider $\mathcal{W}_h = \mathcal{P}_{0,h}$, then matrices $\mathbf{B}$ and $\mathbf{M}$ are diagonal, so the previous system of equations simplifies to:

$$\mathbf{A}[\boldsymbol{\mu}(t)] = \mathbf{b} \tag{3.18}$$

$$\frac{d}{dt}\boldsymbol{\mu}(t) = \mathbf{D}[\mathbf{u}(t)]\boldsymbol{\mu}(t) \tag{3.19}$$

$$\mathbf{a} \cdot \mathbf{u}(t) = 0 \tag{3.20}$$

$$\boldsymbol{\mu}(0) = \tilde{\boldsymbol{\mu}}_0 \tag{3.21}$$

where the $M \times M$-dimensional diagonal matrix $\mathbf{D}$ and the M-dimensional vector $\tilde{\boldsymbol{\mu}}_0$ are given by:

$$D_{k,k}[\mathbf{u}(t)] = \frac{1}{|T_k|}\int_{T_k}\left(\left|\sum_{i=1}^{N} u_i(t)\nabla\varphi_i\right| - 1\right)dx$$

$$\tilde{\mu}_{0_k} = \frac{1}{|T_k|}\int_{T_k}\mu_0 dx$$

where $|T_k|$ is the measure of the element T_k and $\tilde{\boldsymbol{\mu}}_0$ represents the L^2-projection of $\boldsymbol{\mu}_0$ on the triangles of $\mathcal{T}_h$.

Time discretization

In order to solve the DAE system (Equations (3.15)-(3.17)) or the system made of Equation (3.18)-(3.21) we have to define a discretization in time using either forward or backward Euler scheme. We denote with Δt_k the time-step size, so that $t_{k+1} = t_k + \Delta t$ and $(\mathbf{u}^k, \boldsymbol{\mu}^k) = (\mathbf{u}(t_k), \boldsymbol{\mu}(t_k))$. Then the approximate solutions at time t_k can be written as:

$$u_h^k(x) = \sum_{i=1}^{N} u_i^k \varphi_i(x) \qquad \mu_h^k(x) = \sum_{l=1}^{M} \mu_l^k \psi_l(x)$$

Now we are going to analyze two different cases: $\mu_h(t,\cdot) \in \mathcal{P}_{1,h}$ and $\mu_h(t,\cdot) \in \mathcal{P}_{0,h}$.

Case 1: $\mu_h(t,\cdot) \in \mathcal{P}_{1,h}$

The forward Euler Scheme yields:

$$\begin{aligned}
&\mathbf{A}[\boldsymbol{\mu}^k]\mathbf{u}^k = \mathbf{b}\\
&\mathbf{a}\cdot\mathbf{u}^k = 0\\
&\boldsymbol{\mu}^{k+1} = (I + \Delta t_k \mathbf{M}^{-1}\mathbf{B}[\mathbf{u}^k])\boldsymbol{\mu}^k\\
&\boldsymbol{\mu}^0 = \mathbf{M}^{-1}\boldsymbol{\mu}_0
\end{aligned}$$

When backward Euler is employed, we have to solve:

$$\begin{aligned}
&\mathbf{A}[\boldsymbol{\mu}^{k+1}]\mathbf{u}^{k+1} = \mathbf{b}\\
&\mathbf{a}\cdot\mathbf{u}^{k+1} = 0\\
&\mathbf{M}\boldsymbol{\mu}^{k+1} = \mathbf{M}\mu^k + \Delta t_k \mathbf{B}[\mathbf{u}^{k+1}]\boldsymbol{\mu}^{k+1}\\
&\boldsymbol{\mu}^0 = \mathbf{M}^{-1}\boldsymbol{\mu}_0
\end{aligned}$$

Case 2: $\mu_h(t,\cdot) \in \mathcal{P}_{0,h}$

The forward Euler Scheme yields:

$$\begin{aligned}
&\mathbf{A}[\boldsymbol{\mu}^k]\mathbf{u}^k = \mathbf{b}\\
&\mathbf{a}\cdot\mathbf{u}^k = 0\\
&\boldsymbol{\mu}^{k+1} = (I + \Delta t_k \mathbf{D}[\mathbf{u}^k])\boldsymbol{\mu}^k\\
&\boldsymbol{\mu}^0 = \tilde{\boldsymbol{\mu}}_0
\end{aligned}$$

while the backward Euler scheme gives us the following system to solve:

$$\begin{aligned}
&\mathbf{A}[\boldsymbol{\mu}^{k+1}]\mathbf{u}^{k+1} = \mathbf{b}\\
&\mathbf{a}\cdot\mathbf{u}^{k+1} = 0\\
&\boldsymbol{\mu}^{k+1} = \boldsymbol{\mu}^k + \Delta t_k(\mathbf{D}[\mathbf{u}^{k+1}]\boldsymbol{\mu}^{k+1})\\
&\boldsymbol{\mu}^0 = \tilde{\boldsymbol{\mu}}_0
\end{aligned}$$

where the non linearity is solved by a Newton scheme. We can note immediately that the matrix $(I - \Delta t_k \mathbf{D})$ is diagonal, so we can compute its inverse. The stopping criteria is given again by $\rho(\mu_h^{m+1,k+1}, \mu_h^{m,k+1}) \leq \tau_{NL}$ or $m > m_{MAX}$.

Newton scheme

We would like to solve the following sequence of non-linear algebraic equations for $(\boldsymbol{u}^{k+1}, \boldsymbol{\mu}^{k+1})$:

$$\begin{aligned}
\boldsymbol{A}(\boldsymbol{\mu}^{k+1})\boldsymbol{u}^{k+1} &= b\\
\boldsymbol{\mu}^{k+1} &= \boldsymbol{\mu}^k + \Delta t_k(G(\boldsymbol{u}^{k+1})[\boldsymbol{\mu}^{k+1}]^\alpha - \mu^{k+1})
\end{aligned}$$

where the positive definite matrix $\boldsymbol{A}(\boldsymbol{\mu})$ and the diagonal matrix $\mathbf{G}(\mathbf{u})$ are given by:

$$\boldsymbol{A}_{i,j}(\boldsymbol{\mu}) = \sum_E \mu_E \sum_{e\in E} \boldsymbol{\Gamma}^e_{i,j} \quad \boldsymbol{\Gamma}^e_{i,j} = \int_{c_e} \nabla\varphi_i \cdot \nabla\varphi_j dx$$

$$\mathbf{G}(\mathbf{u}) = \frac{\sum_{c_e\in C_E}\int_{c_e} |\nabla u_h|\, dx}{|C_E|^{-1}}$$

We restate the nonlinear system to be solved at each time step k as the problem of finding the zero z of the function:

$$f(z) = \begin{pmatrix} f_u(\boldsymbol{u}, \boldsymbol{\mu}) \\ f_\mu(\boldsymbol{u}, \boldsymbol{\mu}) \end{pmatrix} = \begin{pmatrix} A(\boldsymbol{\mu})\boldsymbol{u} - b \\ \boldsymbol{\mu} - \Delta t_k(\mathrm{diag}[G(\mathbf{u}^{k+1})][\boldsymbol{\mu}^\alpha] - [\boldsymbol{\mu}]) - \boldsymbol{\mu}^k \end{pmatrix} = 0$$

Denoting with m the nonlinear iteration index, Newton method for finding the zero of the above function can be written as:

$$J(f(\mathbf{z}^m))\mathbf{s} = -f(\mathbf{z}^m)$$
$$\mathbf{z}^{m+1} = \mathbf{z}^m + \mathbf{s}$$

The Jacobian matrix J is given by:

$$J(\boldsymbol{u}, \boldsymbol{\mu}) = \begin{pmatrix} \mathbf{A}(\boldsymbol{\mu}) & \mathbf{B}^T(\boldsymbol{u}) \\ -\Delta t_k \mathbf{D}_1(\boldsymbol{\mu})\mathbf{C}(\boldsymbol{u}) & \mathbf{D}_2(\boldsymbol{u}, \boldsymbol{\mu}) \end{pmatrix}$$

where the diagonal matrices $\mathbf{D}_1$ and $\mathbf{D}_2$ and the matrices $\mathbf{B}$ and $\mathbf{C}$ are given by:

$$(\mathbf{D}_1)_{E,E} = \mu_E^\alpha / |C_E| \quad (\mathbf{D}_2)_{E,E} = 1 - \Delta t_k(\alpha \mu_E^{\alpha-1} G_E(\boldsymbol{u}) - \mu_E^{\alpha-1})$$

$$B_{E,i} = \int_{C_E} \nabla u_h \cdot \nabla \varphi_i dx$$

$$C_{E,i} = \sum_{c_e \in C_E} \int_{c_e} |\nabla u_h|^{-1} \nabla u_h \cdot \varphi_i dx$$

Each iteration requires the solution of the linear system:

$$\begin{aligned} \boldsymbol{A}(\boldsymbol{\mu})\boldsymbol{s}_u + \mathbf{B}^T(\boldsymbol{u})\boldsymbol{s}_\mu = -c_u &= -(\boldsymbol{A}(\boldsymbol{\mu}) - \boldsymbol{b}) \\ -\Delta t_k D_1(\boldsymbol{\mu})\boldsymbol{B}(\boldsymbol{u})\boldsymbol{s}_u + D_2(\boldsymbol{u}, \boldsymbol{\mu})\boldsymbol{s}_\mu = -c_\mu &= -((\boldsymbol{\mu} - \Delta t_k(\boldsymbol{G}(\boldsymbol{u})(\boldsymbol{\mu})^\alpha - \boldsymbol{\mu})) - \boldsymbol{\mu}^k) \end{aligned}$$

Now since $\boldsymbol{D}_2$ is diagonal, we can apply its inverse in second equation obtaining:

$$\boldsymbol{M}(\boldsymbol{u}, \boldsymbol{\mu})s_u = \boldsymbol{B}^T \boldsymbol{D}_2^{-1} c_\mu - c_u$$

$$\boldsymbol{s}_\mu = \boldsymbol{D}_2^{-1}(-c_\mu + \Delta t_k \boldsymbol{D_1} \boldsymbol{B} \boldsymbol{s}_u)$$

where the symmetric matrix $\boldsymbol{M}$ can be written as:

$$\boldsymbol{M} = \boldsymbol{A} + \Delta t_k \boldsymbol{B}^T \boldsymbol{D_2}^{-1} \boldsymbol{D}_1 \boldsymbol{B}$$

Moreover, for Δt_k small enough it is also positive definite.

Solution of the linear system

We need to solve a large sparse symmetric linear system positive semi-definite at each Newton iteration. It has this property because there are homogeneous Neumann boundary conditions. The system is solved by a preconditioned conjugate gradient method (PCG) because we are solving a sequence of slightly varying linear systems, so at each system solution we are able to obtain additional data to solve the next linear system in a more efficient way. Moreover, using PCG let us to cope more easily with the near singularity of the stiffness matrix than using a direct solver.
The convergence of the PCG iteration is achieved when the Euclidean norm of the residual relative to the initial residual norm is smaller than the tolerance τ_{CG}. The starting point of our iterations is u_h^k, i.e. the solution at the previous time step, and the preconditioner is an incomplete Cholesky factorization with no fill-in.
In [12] we can find also some numerical experiments about the convergence of the system to closed-form and literature solutions, together with a short analysis on the computational cost.

3.3 Extension of DMK equations to the BTP

We have already seen that the numerical solution of the system of equations written in Problem 10 is a good approximation of the solution of OTP. Now we would like to investigate on a modified system of equations that allows us to obtain a good approximation of the solution of BTP. In this whole section we're going to use the same arguments of [12] and [24]. The authors of [12] have not succeeded into finding an analytical proof of the equivalence between BTP and a suitable system of equations, but their numerical results seem to support this thesis.

Problem 12 *(Extended DMK Problem)*
Given two forcing functions $f^{\pm} : \Omega \to \mathbb{R}$, continuous analogues of the function f of Problem 9, Extended DMK Problem is to find a pair of functions $(\mu, u) : [0, \infty] \times \Omega \to \mathbb{R}^+ \times \mathbb{R}^d$ that satisfies the following equations, complemented by zero Neumann boundary conditions:

$$-\operatorname{div}(\mu(t,x)\nabla u(t,x)) = f^+(x) - f^-(x) \tag{3.22}$$

$$\partial_t \mu(t,x) = [\mu(t,x)\,|\nabla u(t,x)|]^{\beta} - \mu(t,x) \tag{3.23}$$

$$\mu(0,x) = \mu_0(x) > 0 \tag{3.24}$$

where $\partial_t \mu$ and $\nabla = \nabla_x$ indicates partial differentiation with respect to time and spacial gradient, respectively.

Remark 13 *If we consider $\beta = 1$ in Equation (3.23), we obtain exactly Problem 10 where $f(x) = f^+(x) - f^-(x)$, $\forall x \in \Omega$.*

Conjecture 4 *Assuming existence and uniqueness of a solution of the equations of Problem 12, the solution pair $(\mu(t,x), u(t,x))$ converges toward a steady state configuration $(\mu^*(x), u^*(x))$, as it happens in the case $\beta = 1$.*

The solutions of the system of equations in Problem 12 have a very different behavior depending on the exponent β of Equation (3.23).

Conjecture 5 *When $0 < \beta < 1$, the solution pair $(\mu(t,x), u(t,x)$ tends to the state $(|\nabla u_p|^{p-2}, u_p)$, depending on the exponent:*

$$p = \frac{2-\beta}{1-\beta}$$

where u_p is the solution of the p-Poisson equation, with forcing term $f = f^+ - f^-$. (See Proposition 6 for further details on p-Poisson equation).

Remark 14 *If $\beta \to 1$ or $\beta \to 0$, we obtain the cases described in the previous sections in good agreement with Proposition 6 and 3 respectively.*

A proof of this conjecture can be found in Chapter 3 of [12]. We are not going to report all the details, because we are more interested about the case of $\beta > 1$. In this case we are not able to identify a formal connection between Problem 12 and BTP but we are going to show some intuitions about this relation.
We are only interested on the asymptotic behavior of $(\mu(t,x), u(t,x))$, solution of the system presented in Problem 12, so we can assume existence and uniqueness of this solution pair for every $t \geq 0$. Now we are able to define the following Lyapunov-candidate function $\mathcal{L}_\beta(\mu)$ similarly to the case $\beta = 1$:

$$\mathcal{L}_\beta(\mu) := \mathcal{E}_f(\mu) + \mathcal{M}_\beta(\mu) \tag{3.25}$$

where:

$$\mathcal{E}_f(\mu) := \frac{1}{2}\int_\Omega \mu \left|\nabla u(\mu)\right|^2 dx \qquad \mathcal{M}_\beta(\mu) := \begin{cases} \frac{1}{2}\int_\Omega \ln(\mu) & \text{if } \beta = 2 \\ \\ \frac{1}{2}\int_\Omega \frac{\beta}{2-\beta}\mu^{\frac{(2-\beta)}{\beta}} & \text{otherwise} \end{cases}$$

Proposition 19 *Assume that a solution pair $(\mu(t,x), u(t,x))$ of the system of equations in Problem 12 exists and is $\mathcal{C}^1$-regular in time. Then the*

derivative along the $\mu(t)$-trajectory of the candidate-Lyapunov functional $\mathcal{L}_\beta$ is given by:

$$\frac{d}{dt}(\mathcal{L}_\beta(\mu(t))) =$$
$$-\frac{1}{2}\int_\Omega \mu(t)^\beta \left(|\nabla u(\mu(t))|^\beta - (\mu^{\frac{1-\beta}{\beta}}(t))^\beta\right)\left(|\nabla u(\mu(t))|^2 - (\mu^{\frac{1-\beta}{\beta}}(t))^2\right) dx$$

Proof: We're using the same proof of [12].

$$\begin{aligned}\frac{d}{dt}\mathcal{L}(\mu(t)) &= -\frac{1}{2}\int_\Omega \partial_t\mu(t)\left(|\nabla u(t)|^2 - \mu^{\frac{2-2\beta}{\beta}}\right) dx \\ &= -\frac{1}{2}\int_\Omega \left([\mu(t)\,|\nabla u(t)|]^\beta - \mu(t)\right)\left(|\nabla u(t)|^2 - \mu^{2\frac{1-\beta}{\beta}}\right) dx \\ &= -\frac{1}{2}\int_\Omega \mu(t)^\beta \left(|\nabla u(\mu(t))|^\beta - (\mu^{\frac{1-\beta}{\beta}}(t))^\beta\right)\left(|\nabla u(\mu(t))|^2 - (\mu^{\frac{1-\beta}{\beta}}(t))^2\right) dx\end{aligned}$$

where in the second equality we used Equation (3.23). □

Corollary 5 *$\frac{d}{dt}\mathcal{L}(\mu(t))$ is decreasing.*

Proof: If we set $g_1(t,x) := |\nabla u(t,x)|$ and $g_2(t,x) := \mu^{\frac{1-\beta}{\beta}}(t,x)$, we obtain:

$$\frac{d}{dt}\mathcal{L}(\mu(t)) = -\frac{1}{2}\int_\Omega \mu(t)^\beta (g_1(t,x)^\beta - g_2(t,x)^\beta)(g_1(t,x)^2 - g_2(t,x)^2)dx \leq 0$$

This holds because the integrand is always non-negative. □

Remark 15 *Formally, the time derivative of $\mathcal{L}_\beta(\mu(t))$ is equal to zero if the following equations are satisfied:*

$$\begin{cases} -\operatorname{div}(\mu^*\nabla u^*) = f^+ - f^- \\ \\ \mu^* = |\nabla u^*|^{\frac{\beta}{1-\beta}} \end{cases} \tag{3.26}$$

The first equation is Equation (3.22)*, while the second one is equivalent to set $\partial_t\mu(t) = 0$ in Equation* (3.23)*.*

Remark 16 *We can see immediately how Equation* (3.26) *can be linked to the following p-Poisson equation:*

$$-\operatorname{div}(|\nabla u_p|^{p-2}\,\nabla u_p) = f^+ - f^-$$

where $p - 2 = \frac{\beta}{1-\beta}$.

Now we are enunciating some properties without their proofs (See [12] to find them). We need them to prove the following Proposition.

Proposition 20 *Consider $\Omega \subset \mathbb{R}^d$ an open, bounded, connected and convex domain with smooth boundary. Take two non-negative measures f^+ and f^- on Ω such that $df^+(\Omega) = df^-(\Omega)$. Assume that the forcing terms f^+ and f^- admit L^q-densities with $1 < q < +\infty$. Then the following equivalence holds:*

$$\min_{u \in W^{1,p}(\Omega)} \int_\Omega \left(\frac{1}{p} |\nabla u|^p - fu \right) dx = \max_{v \in [L^q(\Omega)]^d} \left\{ - \int_\Omega \frac{|v|^q}{q} dx \ : \ \mathrm{div}(v) = f \right\}$$

where $f = f^+ - f^-$ and p is the Hölder-conjugate exponent of q. The solution u_p of the left-hand side problem and the solution $\bar{v}$ of the right-hand side problem satisfy the following relation:

$$\bar{v} = - |\nabla u_p|^{p-2} \nabla u_p$$

Lemma 8 *Consider Ω an open, bounded, convex and connected domain in $\mathbb{R}^d$ with smooth boundary and $\mu \in \mathcal{M}_+(\Omega)$, $f \in \mathcal{M}(\Omega)$ with zero mean, then the following equality holds:*

$$\mathcal{E}_f(\mu) = - \sup_{\xi \in [L^2_\mu(\Omega)]^d} \left\{ - \int_\Omega |\xi|^2 \mu dx \ : \ \mathrm{div}(\xi \mu) = f \right\} \tag{3.27}$$

Remark 17 *Since $\mathcal{M}_\beta(\mu)$ does not depend on the variable u in Equation (3.26), if we add it to both sides of Equation (3.27), we obtain $\mathcal{L}_\beta(\mu)$ on the left side.*

Proposition 21 *Let $q = 2 - \beta$ and $P(\beta) = \frac{2-\beta}{\beta}$. Then the following inequality holds:*

$$\inf_{v \in [L^q(\Omega)]^d} \left\{ \int_\Omega \frac{|v|^q}{q} dx \ : \ \mathrm{div}(v) = f \right\} \leq \inf_{\mu \in L_+^{P(\beta)}(\Omega)} \mathcal{L}_\beta(\mu) \tag{3.28}$$

Proof: We can rewrite $\mathcal{L}_\beta(\mu)$ as it follows:

$$\mathcal{L}_\beta(\mu) = \inf_{\xi \in [L^2_\mu(\Omega)]^d} \{ \Theta(\mu, \xi) \ : \ \mathrm{div}(\xi \mu) = f \} \quad \forall \mu \in L_+^{P(\beta)}(\Omega) \tag{3.29}$$

where:

$$\Theta(\mu, \xi) := \frac{1}{2} \left[\int_\Omega |\xi|^2 \mu dx + \int_\Omega \frac{\beta}{2 - \beta} \mu^{\frac{2-\beta}{\beta}} dx \right]$$

For any pair $(\mu, \xi) \in \left(L_+^{P(\beta)}(\Omega), [L^2_\mu(\Omega)]^d\right)$ the following inequalities holds by using Hölder inequality, where $\frac{2}{q}$ and $\frac{2}{2-q}$ are the conjugated exponents:

$$\int_\Omega |\xi\mu|^q \, dx = \int_\Omega |\xi|^q \, \mu^{\frac{q}{2}} \mu^{\frac{q}{2}} dx \leq \frac{q}{2} \int_\Omega |\xi|^2 \, \mu dx + \frac{2-q}{2} \int_\Omega (\mu^{\frac{q}{2}})^{\frac{2}{2-q}} dx$$

If we set $\frac{q}{2-q} = \frac{2-\beta}{\beta}$ (and so $q = 2-\beta$) and we divide by q the previous inequality, we get:

$$\int_\Omega \frac{|\xi\mu|^{(2-\beta)}}{(2-\beta)} dx \leq \frac{1}{2} \int_\Omega |\xi|^2 \, \mu dx + \frac{1}{2} \int_\Omega \frac{\beta}{2-\beta} \mu^{\frac{2-\beta}{\beta}} dx = \Theta_\beta(\mu, \chi)$$

which holds for all $\mu \in L_+^{P(\beta)}(\Omega)$ and for all $\xi \in [L^2_\mu(\Omega)]^d$.
Now, if we take two infima on both sides, the first one over $\xi \in [L^2_\mu(\Omega)]^d$ and the second one over $\mu \in L_+^{P(\beta)}(\Omega)$, using the previous Lemma, we get:

$$\inf_{\mu \in L_+^{P(\beta)}(\Omega)} \left\{ \inf_{\xi \in [L^2_\mu(\Omega)]^d} \left\{ \int_\Omega \frac{|\xi\mu|^{(2-\beta)}}{(2-\beta)} dx \ : \ \mathrm{div}(\xi\mu) = f \right\} \right\} \leq \inf_{\mu \in L_+^{P(\beta)}(\Omega)} \mathcal{L}_\beta(\mu)$$

Moreover, the following inequality holds:

$$\inf_{v \in [L^q_+(\Omega)]^d} \left\{ \int_\Omega \frac{|v|^q}{q} dx \ : \ \mathrm{div}(v) = f \right\} \leq$$

$$\inf_{\mu \in L_+^{P(\beta)}(\Omega)} \left\{ \inf_{\xi \in [L^2_\mu(\Omega)]^d} \left\{ \int_\Omega \frac{|\xi\mu|^{(2-\beta)}}{(2-\beta)} dx \ : \ \mathrm{div}(\xi\mu) = f \right\} \right\}$$

so we have obtained the thesis. □

Remark 18 *In the case $0 < \beta < 1$ we can show the uniqueness of the minimum μ^*_β, due to the strictly convexity of $\mathcal{L}_\beta$, but this argument does not hold for the case $1 < \beta < 2$.*

We are going to analyze the case $1 < \beta < 2$ now. As we already said, in this case it's not possible to find an unique minimizer for $\mathcal{L}_\beta(\mu)$, but we can observe how this formulation seems similar to the BTP formulated by Xia (see Section 1.5.2), where the exponent q plays the role of the branching exponent α. There is an important difference between Xia's formulation and the left-hand side of Equation (3.28): in the first one we are integrating with respect to the 1-dimensional Hausdorff measure, while in the second one we are using Lebesgue measure. Nevertheless, the numerical experiments made in [12] seem to support the equivalence of these two formulations, so we can enunciate the following:

Conjecture 6 *If $\beta > 1$, the solution $(\mu(t), u(t))$ of Equations (3.22)-(3.24) admits an equilibrium point (μ^*_β, u^*_β) depending on the initial condition μ_0. Moreover, this solution is a minimum of the Lyapunov-candidate functional $\mathcal{L}_\beta$.*

We can also observe that, since $p = (2-\beta)/(1-\beta) < 0$, the steady state should be solution of a p-Poisson equation with a negative exponent p and the only reference about a solution of this kind of equation in the literature can be found in Xia's work on BTP, but they are working on a graph structure. Lastly, we want to highlight that exponents p and $q = 2-\beta$ are Hölder-conjugate.

Remark 19 *One possible way to reconcile the two different integration measures could be an approach inspired by Modica-Mortola idea. In [24] there is a proof of the convergence for the BTP, but only in the 2-Dimensional case.*

3.4 Numerical approach for Extended DMK equations

We're using a combination of the $\mathcal{P}_{1,h/2}$-$\mathcal{P}_{0,h}$ spatial discretization with the forward Euler scheme. We can approximate the solution pair $(\mu(t,x), u(t,x))$ of Equation (3.22) with the pair $(\mu_h(t,x), u_h(t,x))$ such that:

$$u_h(t,x) = \sum_{i=1}^{N} u_i(t)\varphi_i(x) \quad \varphi \in \mathcal{P}_1(\mathcal{T}_{h/2})$$

$$\mu_h(t,x) = \sum_{k=1}^{M} \mu_k(t)\psi_k(x) \quad \psi \in \mathcal{P}_0(\mathcal{T}_h)$$

After having applied the same arguments of Section 3.2, we obtain the following sequence of linear systems when using forward Euler time stepping:

$$\mathbf{A}[\mu^k]\mathbf{u}^k = b \tag{3.30}$$

$$\boldsymbol{\mu}^{k+1} = \boldsymbol{\mu}^k + \Delta t_k \left[\mathbf{B}_\beta[\mathbf{u}^k](\boldsymbol{\mu}^k)^\beta - \boldsymbol{\mu}^k\right] \tag{3.31}$$

where $\mathbf{A}[\boldsymbol{\mu}^k]$ and $\mathbf{B}_\beta[\mathbf{u}^k]$ are the stiffness matrix associate to $\boldsymbol{\mu}^k$ and the matrix defining the norm of the gradient of $u_h(t^k, x)$ raised to the power β, respectively.
As we did in the case $\beta = 1$, we started from the projected initial data μ^0_h and we iterate until:

$$\mathrm{var}(\mu^k_h) := \frac{\left|\left|\mu^{k+1}_h - \mu^k_h\right|\right|_{L^2(\Omega)}}{\Delta t^k_k \left|\left|\mu^k_h\right|\right|_{L^2(\Omega)}} < \tau_T$$

where τ_T is a fixed threshold. Moreover, in order to avoid singularities, we impose also a lower bound of 10^{-10} for $\mu_h(t,x)$. The system is solved again via Preconditioned Conjugate Gradient (PCG). For further details about the preconditioner, see Chapter 4 of [12], where some strategies are studied in order to solve this system of equations efficiently.

Chapter 4

Numerical Simulations

As we have already seen in the previous chapters, the notion of branching angles is very important in the biological systems, such as blood vessels, and are considered as one of the fundamental invariants of a spatially distributed network structure. In this chapter we study the branching angles that arises from the numerical solution of the DMK. First, we have to show a relation between the exponent β of Extended DMK model (see Problem 12 in Chapter 3) and the branching angles found by Woldenberg (see Table 2.2 in Chapter 2). To help the reader, we report here the formulation seen in the previous chapters that are going to be used for our purpose.

Problem 12 (Extended DMK Model) (repeated)
Given two forcing functions $f^{\pm} : \Omega \to \mathbb{R}$, continuous analogues of the function f of Problem 9, Extended DMK Problem is to find a pair of functions $(\mu, u) : [0, \infty] \times \Omega \to \mathbb{R}^+ \times \mathbb{R}^d$ that satisfies the following equations, complemented by zero Neumann boundary conditions:

$$-\operatorname{div}(\mu(t,x)\nabla u(t,x)) = f^+(x) - f^-(x) \tag{3.22}$$

$$\partial_t \mu(t,x) = [\mu(t,x)\,|\nabla u(t,x)|]^{\beta} - \mu(t,x) \tag{3.23}$$

$$\mu(0,x) = \mu_0(x) > 0 \tag{3.24}$$

where $\partial_t \mu$ and $\nabla = \nabla_x$ indicates partial differentiation with respect to time and spacial gradient, respectively.

Corollary 3 (Woldenberg Angles [31] - [32]) (repeated)
The measure of a bifurcation angle of an arterial network is given by Table 2.2 (reported below) where x is the exponent of the generalized Murray's Law $f = kr^x$ (see Equation (2.9)), where f and r are, respectively, the flow and the radius of a blood vessel and k is a constant depending only on the geometry of the vessel, and $\alpha = r_2/r_1 \in]0, 1[$ is the radii ratio.

Optimality Principle	$\cos(\theta_1)$	$\cos(\theta_2)$	$\cos(\theta)$
Min. Surface	$\frac{(1+\alpha^x)^{2/x}+1-\alpha^2}{2(1+\alpha^x)^{1/x}}$	$\frac{(1+\alpha^x)^{2/x}-1+\alpha^2}{2\alpha(1+\alpha^x)^{1/x}}$	$\frac{(1+\alpha^x)^{2/x}-1-\alpha^2}{2\alpha}$
Min. Volume	$\frac{(1+\alpha^x)^{4/x}+1-\alpha^4}{2(1+\alpha^x)^{2/x}}$	$\frac{(1+\alpha^x)^{4/x}-1+\alpha^4}{2\alpha(1+\alpha^x)^{2/x}}$	$\frac{(1+\alpha^x)^{4/x}-1-\alpha^4}{2\alpha^2}$
Min. Pumping Power	$\frac{(1+\alpha^x)^{4-8/x}+1-\alpha^{4x-8}}{2(1+\alpha^x)^{2-4/x}}$	$\frac{(1+\alpha^x)^{4-8/x}-1+\alpha^{4x-8}}{2\alpha^{2x-4}(1+\alpha^x)^{2-4/x}}$	$\frac{(1+\alpha^x)^{4-8/x}-1-\alpha^{4x-8}}{2\alpha^{2x-4}}$
Min. Drag Force	$\frac{(1+\alpha^x)^{2-4/x}+1-\alpha^{2x-4}}{2(1+\alpha^x)^{1-2/x}}$	$\frac{(1+\alpha^x)^{2-4/x}-1+\alpha^{2x-4}}{2\alpha^{x-2}(1+\alpha^x)^{1-2/x}}$	$\frac{(1+\alpha^x)^{2-4/x}-1-\alpha^{2x-4}}{2\alpha^{x-2}}$

Definition 5 (Xia's Transport path and its energy) (repeated)
Let μ^+ and μ^- be two positive Radon measures with equal mass in a compact convex set $X \subset \mathbb{R}^N$. A vector measure T on X with values in $\mathbb{R}^N$ is called a transport path from μ^+ to μ^- if there exist two sequences μ_i^-, μ_i^+ of finite atomic measures with equal mass and a sequence of finite graphs G_i irrigating (μ_i^+, μ_i^-) such that $\mu_i^+ \to \mu^+$, $\mu_i^- \to \mu^-$ weakly as measures and $G_i \to T$ as vector measures. The energy of T is defined by:

$$M^\alpha(T) := \inf_A \liminf_{i\to\infty} M^\alpha(G_i) \tag{4.1}$$

where:

$$A := \{(\mu_i^+, \mu_i^-, G_i) \ : \ \text{approximating sequences to T}\}$$

We used also the following notation to indicate the cost function:

$$M^\alpha(\mu^+, \mu^-) := \inf\{M^\alpha(T) \ : \ \text{T is a transport path from } \mu^+ \text{ to } \mu^-\}$$

At last, we recall also that there are also some numerical experiments that seem to link Xia's minimization problem to the following minimization problem:

$$\inf_{v\in[L^q(\Omega)]^d} \left\{ \int_\Omega \frac{|v|^q}{q} dx \ : \ \mathrm{div}(v) = f \right\} \tag{4.2}$$

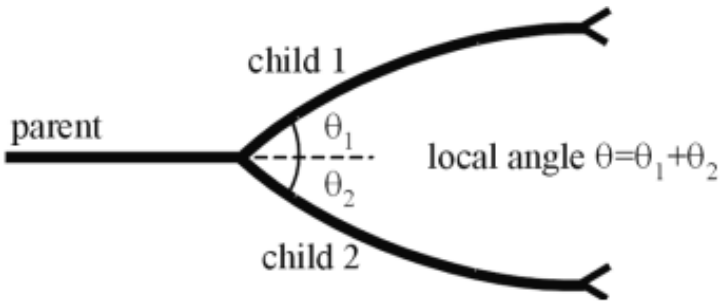

Proposition 22 *(Angles relations)*
If the left hand-side of Equation (4.2) *and Xia's formulation (see Equation* (1.16)*) are equivalent, then the following relations between Woldenberg angles in Table 2.2 and the exponent β in Problem 12 hold:*

1. *if the optimality principle is the minimum volume, then:*

$$2-\beta=\frac{2}{x} \quad \Longrightarrow \quad x=\frac{2}{2-\beta}$$

2. *if the optimality principle is the minimum surface, then:*

$$2-\beta=\frac{1}{x} \quad \Longrightarrow \quad x=\frac{1}{2-\beta}$$

3. *if the optimality principle is the minimum pumping power, then:*

$$2-\beta=\frac{2x-4}{x} \quad \Longrightarrow \quad x=\frac{4}{\beta}$$

4. *if the optimality principle is the minimum drag force, then:*

$$2-\beta=\frac{x-2}{x} \quad \Longrightarrow \quad x=\frac{2}{\beta-1}$$

Proof: Formally, the thesis follows by substituting a in Corollary 7 with $2-\beta$. □

Remark 20 *The previous proof is not rigorous but contains only formal results, because it is based on the Conjecture 6 in which we stated that the exponent β of Problem 12 is equivalent to $2-q$, where q is the exponent of the cost function in Definition 4.1, but we want to highlight once more that there are no proofs of this equivalence, even if there are numerical results which seem to support it. The critical aspect is the difference in the integration measures: in Problem 12 the Lebesgue measure is used, while in Section 1.5.2 Hausdorff measure has been used. Moreover, in Proposition 15 we saw the equivalence of cost functions for the two formulations used and, if these costs are finite, the solutions of the minimization problems coincide. Lastly, in Corollary 4 we saw the relation between the angles in Table 2.2 found by Woldenberg and the angles found by Morel in Lemma 7.*

Corollary 6 *If Murray's Law holds (see Equation* (2.5)*), i.e. if $x=3$ in the previous Proposition, then the exponent β that describes the minimum Volume and minimum Pumping Power cases is $\beta=4/3$, while for the other two cases $\beta=5/3$.*

We want to recall that Murray's Law arises from the hypothesis of having a Pouiseulle flow. The proof of this Corollary is immediate, but it is interesting to see that in all these cases $1 < \beta < 2$, corroborating the hypothesis that the BTP exponent β for the branched part of Problem 12 lies in that interval. Moreover, if the flow is turbulent (i.e. $x = 7/3$), then $1 < \beta < 2$ in that case too, so even in all the intermediate cases in which Generalized Murray's Law hold (see Equation (2.9)) we have a link with the branched cases of Extended DMK model.
Before starting to show some numerical results obtained by applying Extended DMK model to arteries, we want to highlight that DMK acts at a "meso-scale" where laminar flow is fully developed and cannot represent the structure of "middle-size" or large arteries, in which the flow of blood can be a turbulent flow or capillaries where diffusion dominates. Before starting to analyze the numerical results, we would like to highlight the following fact.

Lemma 9 *The measure of the bifurcation angles increases as β increases for every fixed $\alpha = r_2/r_1 \in]0, 1[$.*

We do not report here the proof of this Lemma, as it is a direct consequence of the explicit relation between β and the angles in Table 2.2, we have only to substitute the expressions for x depending on β that can be found in Proposition 22 into Table 2.2 and then we have only to compute the sign of the derivative of a function.

4.1 Numerical Methods

In this section we describe the numerical methods used to measure of the bifurcation angles starting from the DMK model. We need first to build the graph structure from the solution of DMK and then we have to simplify it in order to compute the bifurcation angles more precisely.

DMK solution

In the first phase of our method we have to get the solution of the Extended DMK model described in the previous chapter. After having set the appropriate initial condition, we can proceed as described in Chapter 3. The solution of the problem is a density μ^* in the continuous case, while it is a piecewise constant function in the discrete case. The output is not a network, so it is not useful in order to compute the measure of bifurcation angles. Moreover,

our conjecture is that the distribution of μ is fractal. There is no proof of this fact, but our numerical results seem to support this thesis.
We chose to build a graph from our solution in order to obtain the network structure we are looking for.

Construction and Analysis of Graphs

We describe the method used to recover the graph starting from the solution of the DMK model that we obtained previously. Firstly, we select the triangles in which the value of μ is greater than a certain value μ_{min} that has to be chosen experimentally. Later, we link two of these triangles with a graph edge if they have a common vertex or edge. Clearly, the resulting graph is going to have a high number of redundant nodes and edges that will need to be reduced. This method leads to slightly different configurations when working on a sequence of refined meshes. To minimize these discrepancies we consider also the mid points of the selected triangles edges when we are creating the links, so the number of nodes and edges is even greater than in the previous case. This behavior is caused by the structure of the triangulation of the FEM. This resulting structure is too complex to be useful in the identification of the branching points because the adjacency matrix of this graph has too many non zero entries. Nevertheless, we are able to identify the set of termination nodes of this graph easily. This set is formed by the sources and the leaves of the graph. We tried three different methods in order to simplify the initial graph:

- Firstly, we tried to use the algorithm for the construction of a Steiner tree, which can be found in the documentation of the Networkx package of Python (`https://networkx.github.io/documentation/latest/reference/algorithms/generated/networkx.algorithms.approximation.steinertree.steiner_tree.html`). It needs only a graph and a list of termination nodes as inputs. This information can be obtained easily from the previous graph, so this method seems useful, but the final result was a bit inaccurate in a neighborhood of the bifurcation points. This behavior is caused by the definition of a Steiner tree. The Steiner Tree of a set of termination nodes L of a graph G is a subgraph S of G formed by a minimal spanning tree for every node $n \in L$. We recall that a spanning tree of a graph is a subgraph that is a tree which includes all the vertices of the initial graph and has the minimum possible number of edges.

- Next, we tried to exploit the dynamics of the system to achieve graph simplification: we wanted to analyze the result obtained by solving

the Extended DMK model on the connected components of the graph, in which we would like to transport a mass density from the sources to the leaves. Thus we run again the DMK dynamics on the graph obtained from the FEM mesh. The result of this method was more accurate than the previous one, but its accuracy was not enough for our purposes because there were some errors in the larger branches of the tree, i.e. the branches in which the value of μ is higher.

- Finally, we tried another method to obtain the simplified graph structure. We decided to use Dijkstra's algorithm that finds the shortest path on a graph. We use the graph structure and the algorithm written by [5] that can be found in `https://www.bogotobogo.com/python/python_graph_data_structures.php` and in `https://www.bogotobogo.com/python/python_Dijkstras_Shortest_Path_Algorithm.php`. Dijkstra's algorithm computes the graph distance from a fixed node n_0 to every other nodes in a connected component of a graph G, so we only needed information about the sources of the graph (they will be the starting points n_0) and the edges of the graph. Then we created the simplified graph as a union of the shortest paths between the initial node n_0 and every leaf belonging to the same connected component of n_0. The final result of this method was similar to the second one, but there was a smaller number of errors in large branches, so we decided to use this shortest path method.

Finally, we obtained a tree structure from the initial solution, but this result is not enough to compute the measure of the branching angles, because this tree strongly depends on the mesh, so we have to find a simpler tree which approximates our solution. Firstly, we decided to ignore the branches with a length smaller than a fixed tolerance *tol* (usually 2), because this branches are caused by the initial choice of μ_{min}. We tried four different methods to do this simplification. Before starting the description of the algorithms used, we would like to highlight that we can easily extract some important information from the tree structure. We already knew the sources and the leaves of the tree from the previous steps, but now we can find the bifurcation points easily from the adjacency matrix of the tree; in fact, the bifurcation nodes are the ones with at least three adjacent nodes. The following definition will be used later.

Definition 19 *(Passing Points)*
Consider a graph $G = (V, E)$. We indicate with B_G and T_G the subsets of V containing the bifurcation points of G and its termination points, respectively. We call the set of passing points of G: $V \supset P_G := B_G \cup T_G$.

We say also that two points in the set of passing points are consecutive if they belong to the same path between the source and a leaf and there is no other passing point in this path between them.

Now we are going to describe the methods used to approximate the "Shortest Path" graph:

1. **Minimum Graph Method**
   We consider only a minimal tree, made of the sources, the leaves and the set of bifurcation points

2. **Graph Distance Method**
   We add the additional points if the graph distance between two consecutive nodes is greater than a fixed tolerance d_G

3. **Euclidean Distance Method**
   We select the nodes that have to be added considering the Euclidean distances between two consecutive points in the set of passing points. If this distance is greater than a fixed value d_0, usually between 1 and 3.5, we add some intermediate points between them.

4. **Security Region Method**
   We fix a radius r, small enough. Then we compute the distance d_{p_j} from the segment joining two consecutive passing points a and b for every point p_j in a path between these passing points, where $j = 0, \ldots, m$ and $p_0 = a$, $p_m = b$. If $d_{p_j} > r$, and $d_{p_{j-1}}, d_{p_{j+1}} < r$, and consider also the point p_j in our tree. Indeed, if there are at least two adjacent points that are situated outside the cylinder of radius r and axis the segment ab, we decided to consider only the middle point.

The results obtained by minimum graph method are too inaccurate because it does not consider all the intermediate directions taken by the branch, but it only links the starting and the final points of it, so there could be some huge errors during the computations of the angles. That is the reason why we decided to consider also some intermediate points that are not bifurcations. In the graph distance method we tried different values for the tolerance d_G, but in all the cases the final result was not too accurate, because a small tolerance presented the same kind of errors of the shortest path tree, while a larger one gave us a result similar to the minimal tree described above.
The Euclidean distance method is a bit more accurate than the previous one, but we have to pay attention to the right choice for d_0: if this value is too small, the resulting tree is not too different from the shortest path tree, while, if d_0 is too large, we are obtaining the same problems of the minimal

tree.
The last method was usually the more accurate, so we decided to use this one.
At last we did a final approximation of our tree. We decided to not consider a pair of bifurcation points if their Euclidean distance is smaller than the tolerance *tol* used previously. In this cases we consider only one bifurcation point situated in the mid point of the segment between the two original points.

Angles analysis

Finally, from the resulting tree structure we are able to compute the bifurcation angles. We know the coordinates of each node of our reduced graph and we are able to identify the bifurcation points. So we have only to use the following formula to compute the angle α between two segments:

$$\alpha = \arctan\left(\left|\frac{m_1 - m_2}{1 + m_1 m_2}\right|\right)$$

where m_1 and m_2 are the angular coefficient of the segments between the bifurcation points and the first node. For every simulation, because of all the approximations errors in this sequential procedure, starting from numerical errors in DMK finite element solution to arrive at errors in the graph identification, bifurcation angles are evaluated statistically. Thus we collect our results in histograms (with bins of $5°$) and evaluate their mean, median, standard deviation and skewness.

4.2 Example of the method

In this section we are going to analyze an application of our method. We chose to work with the arterial network of a frog tongue [9]. We can find an illustration of the cardiovascular network of a frog tongue in Figure 4.1. We can also extract easily the arterial network, as shown in Figure 4.2 (we have only to consider the red vessels in Figure 4.1).

Remark 21 *In Figure 4.1 we can observe that there are some loops. Our algorithm is not able to describe behaviors similar to that one, but in [12] there is a conjecture which states that similar loops are created when the forcing is non-stationary. In our simulations we are considering only the case of a forcing function independent from time, even if this hypothesis is not compatible with the irregular heartbeat.*

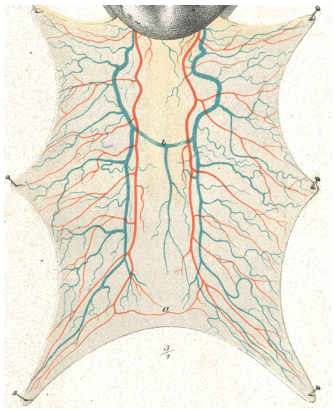

Figure 4.1: Circulatory system of a frog tongue: arteries are drawn in red, while veins are represented in blue. Image taken by [9]

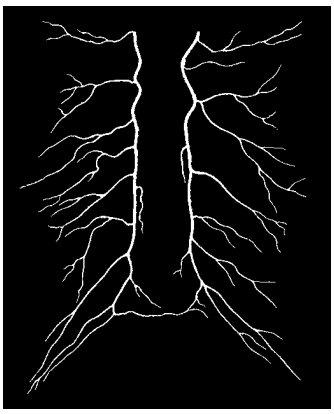

Figure 4.2: Arteries in a frog tongue

Figure 4.1 helps us to identify also the sources and the domain D of the problem. We can see them in Figure 4.3 and in Figure 4.4, respectively. It is

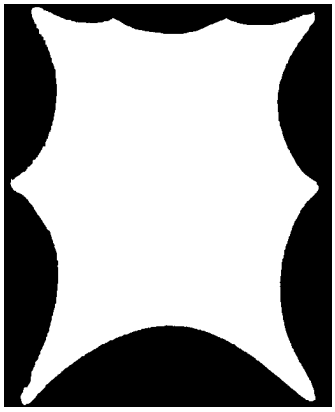

Figure 4.3: Domain D of the problem

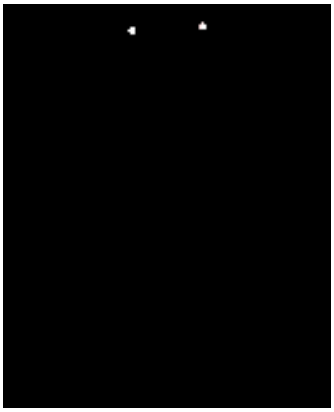

Figure 4.4: Injection points of the problem

reasonable to consider the whole domain D as the sink of our problem. Lastly, we set the initial condition for the density μ as the uniform distribution $\mu_0(x) = 10^{-10}\ \forall x$.
After having chosen the resolution method and its stopping conditions, we can start the simulations. In Figure 4.9 we can observe the dependence of our solutions from the lower threshold μ_{min} of μ. We can see easily that there is a difference of some order of magnitude between the minimum and

the maximum values of μ, so we have to use a logarithmic scale in order to represent μ. If μ_{min} is quite small, as for example in Figure 4.8 and Figure 4.7,

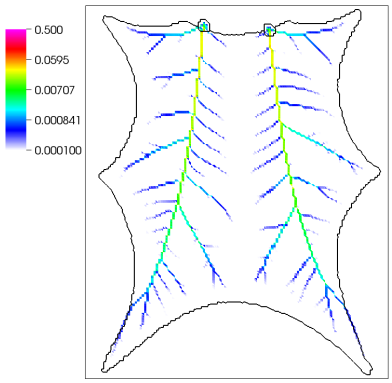

Figure 4.5: $\mu \in [10^{-4}, 0.5]$

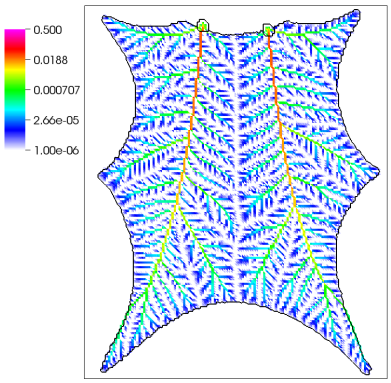

Figure 4.6: $\mu \in [10^{-6}, 0.5]$

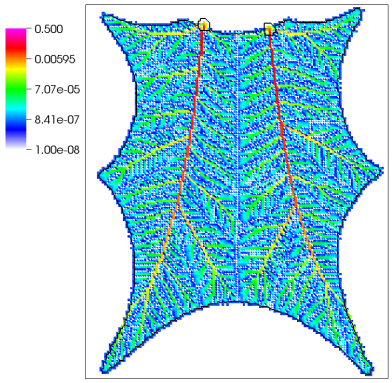

Figure 4.7: $\mu \in [10^{-8}, 0.5]$

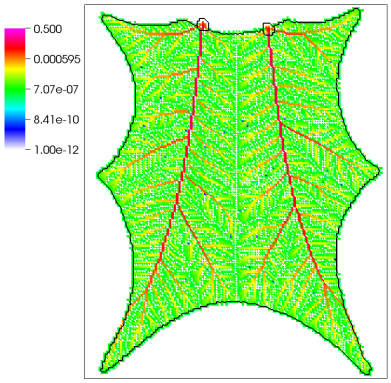

Figure 4.8: $\mu \in [10^{-12}, 0.5]$

Figure 4.9: Examples of graphical representations of the solutions μ of our problem for $\beta = 1.20$ and various lower bounds for μ for the non-refined mesh. The region inside the black contour is the domain D of our problem.

the resulting graphs cover all the domain D, so we have too much information and it is not easy to recover the graph structure and compute the bifurcation angles. Moreover, we can see also that these two figures have a very similar profile, so we can suppose that $\mu_{min} = 10^{-12}$ is a condition too strong. If we raise up the threshold value μ_{min} to 10^{-6}, we obtain a simpler figure than the previous one, but there are too many branches also in this case, as we can

observe in Figure 4.6. Our conjecture on the fractal behavior of the variable μ seems to be satisfied in these three figures. At last, if we raise up μ_{min} again to 10^{-4}, we obtain Figure 4.5. In this last case we can observe how there is a smaller number of branches with respect to the previous cases. Here we could extract easily the graph structure and then we can compute the measure of the branching angles, but the number of branches is too low, so we usually look for a compromise between Figure 4.5 and Figure 4.7. After having set

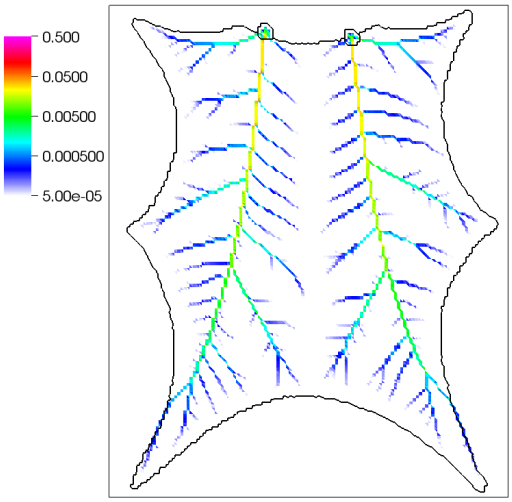

Figure 4.10: Example of solution μ when $\beta = 1.20$ and $\mu_{min} = 5 \cdot 10^{-5}$.

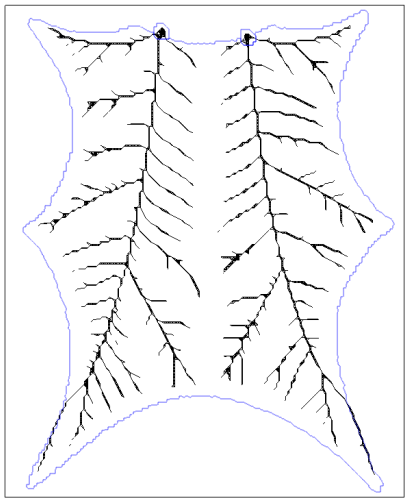

Figure 4.11: Example of graph obtained by the solution μ when $\beta = 1.20$ and $\mu_{min} = 5 \cdot 10^{-5}$.

$\mu_{min} = 5 \cdot 10^{-5}$, in Figure 4.10 we can observe that the number of branches is not too small or too large, so we decided to keep on working with this threshold. The next step is to get a graph structure from the solution shown in the last figure. This graph can be seen in Figure 4.11. We can observe immediately the presence of a number of microscale loops in the graph, as we can see in Figure 4.13. That is the reason why we have to simplify it in order to individuate the bifurcation points. We show here only the "Shortest Path" graph which can be found in Figure 4.12. We can observe how the number of loops is greatly reduced, so we can identify the bifurcation points easily, but the branching angles depend on the initial mesh too much, so we have to simplify the graph again in order to obtain a better accuracy in the measures of the angles. We are going to show all the four methods

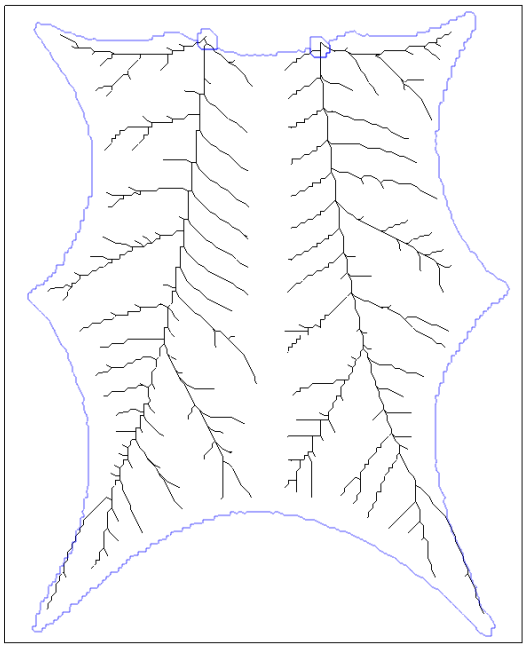

Figure 4.12: Example of "Shortest Path" Graph obtained by the solution μ when $\beta = 1.20$ and $\mu_{min} = 5 \cdot 10^{-5}$.

described in the previous section. In Figure 4.18 we can see the results of the applications of every method. In these figures we have already deleted the smallest branches and joined two near bifurcations points, as we described in the previous section. Figure 4.14 seems a good approximation of Figure 4.12 for our choices of β and μ_{min}, but there are some evident errors, such as on the lower corners of the domain. These errors drive us to look for other ways to approximate the "Shortest Path" graph of Figure 4.12. The tree obtained in Figure 4.16 seems not to be independent enough from the original mesh, so the measures of the angles are quite different from what we can observe in the other cases. Lastly, the results obtained in Figure 4.15 and in Figure 4.17 are very similar and they seem a good compromise between Figure 4.14 and Figure 4.12, so we are using usually one of these methods.
Now we are able to compute the measure of the branching angles. We can see an histogram for every method in Figure 4.23 and a statistical analysis in Table 4.1.

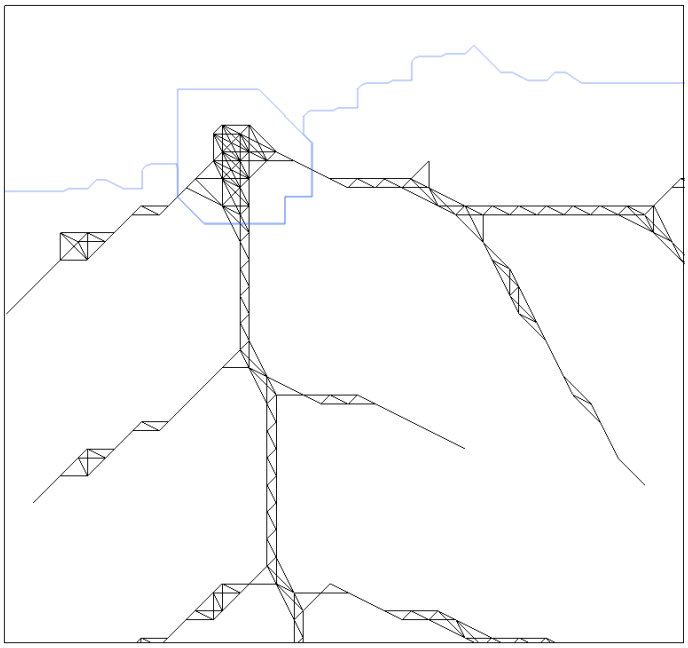

Figure 4.13: Zoom of Figure 4.11 in a region near one of the two injection points: we can easily notice the presence of loops in this graph structure.

We can observe how the Euclidean Distance method and the Security Region method give us very similar results, but the second one seems to have a higher accuracy because the difference between Mean and Median is lesser than in the other case. We can also observe how the method that uses the Graph Distance to add further points give us results very different respect to the other three methods.

The case of the Refined Mesh

Now we are going to show the results obtained when we use the refined mesh for the same exponent $\beta = 1.20$. Figure 4.26 shows us that $\mu_{min} = 10^{-6}$ is not a good choice, because the structure is too complex, as it can be seen in Figure 4.25. $\mu_{min} = 10^{-5}$ seems a good choice (see Figure 4.24), but we decided to use a higher value for μ_{min} due to the high complexity of the graph structure, as we are going to see later. We set $\mu_{min} = 10^{-4}$ and we obtained

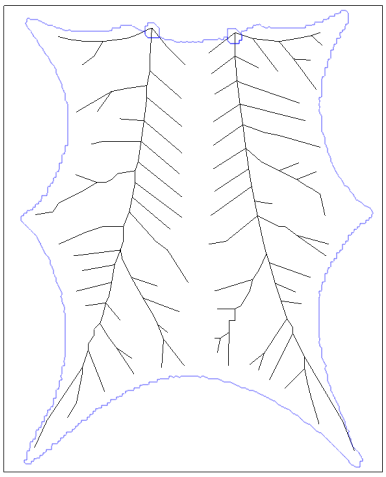

Figure 4.14: Reduced Graph with only sources, leaves and bifurcation points

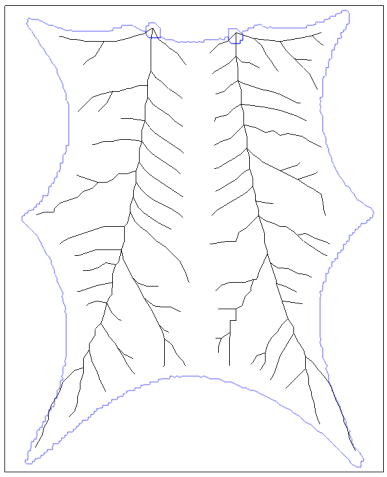

Figure 4.15: Reduced graph with Euclidean distance used for additional points.

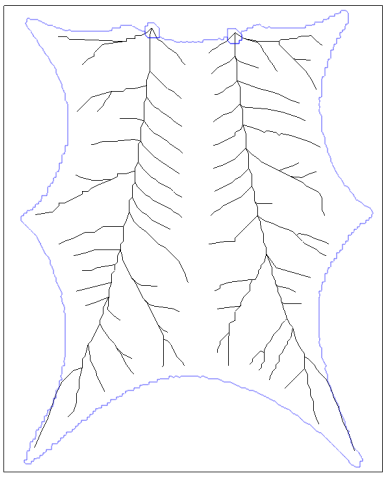

Figure 4.16: Reduced graph with graph distance used for additional points.

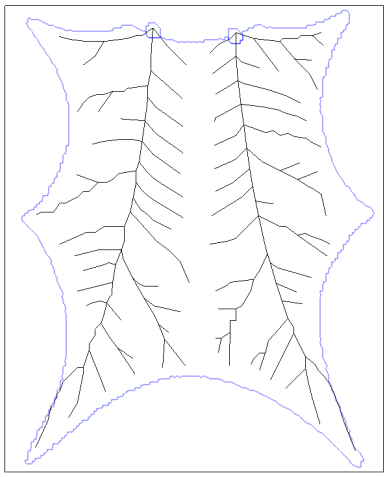

Figure 4.17: Reduced graph with security region used for additional points.

Figure 4.18: Application of the four different reduction methods for the "Shortest Path" Graph in Figure 4.12

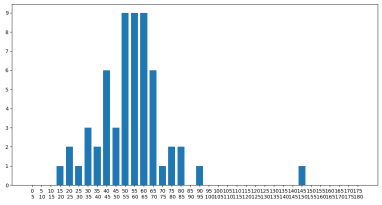

Figure 4.19: Histogram of the measure of the bifurcation angles for reduced Graph with only sources, leaves and bifurcation points (Figure 4.14).

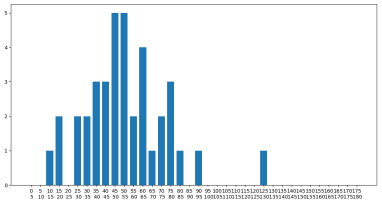

Figure 4.20: Histogram of the measure of the bifurcation angles for reduced graph with Euclidean distance used for additional points (Figure 4.15).

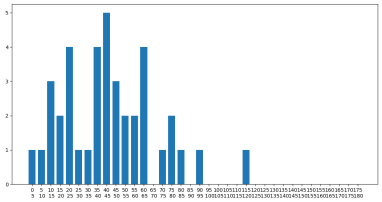

Figure 4.21: Histogram of the measure of the bifurcation angles for reduced graph with graph distance used for additional points (Figure 4.16).

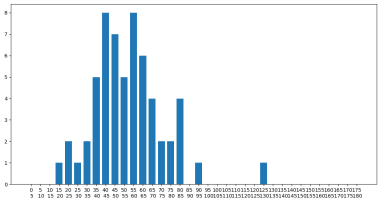

Figure 4.22: Histogram of the measure of the bifurcation angles for reduced graph with security region used for additional points (Figure 4.17).

Figure 4.23: Histograms of the measure of the bifurcation angles for the four different reduction methods for the "Shortest Path" Graph in Figure 4.12

Reduction Type	Mean	Median	Variance	Skewness
Minimal Graph	56 ° 36'	57 ° 42'	336.07	1.67
Euclidean Distance	56 ° 12'	54 ° 00'	441.89	0.70
Graph Distance	49 ° 06'	47 ° 30'	718.45	0.42
Security Region	55 ° 48'	54 ° 36'	355.68	0.82

Table 4.1: Statistical data on the angles of the various reduced graphs for $\beta = 1.20$

the result shown in Figure 4.27. Now we can work as in the previous case and we can extract the graph from Figure 4.27, obtaining Figure 4.28 We can observe immediately how the number of edges and nodes in Figure 4.28 is greater than in Figure 4.11, so it will even be more important than in the previous case to simplify this graph. We used Dijkstra's shortest path algorithm in this case and we obtain what we can see in Figure 4.29. Now we are able to find the reduced trees, using the four methods described previously. Now we can analyze the histograms and the statistical information about the angles in Figure 4.39 and in Table 4.2, respectively.

Reduction Type	Mean	Median	Variance	Skewness
Minimal Graph	55 ° 51'	54 ° 54'	576.16	1.82
Euclidean Distance	56 ° 06'	56 ° 18'	584.88	0.81
Graph Distance	54 ° 21'	60 ° 27'	1117.97	0.01
Security Region	54 ° 39'	51 ° 21'	638.63	1.21

Table 4.2: Statistical data on the angles of the various reduced graphs for $\beta = 1.20$ when the refined mesh has been used.

We can observe easily how the reduction method which uses the graph distance is very inaccurate. The "minimal graph method" seems to have a good accuracy, but, as it happened previously, there are some evident problems in the lower part of the figure, so we decided to not use this method, so we always chose one of the other two methods during the last step of the approximation of the solution μ via graphs.
Before proceeding with the analysis of the results obtained with different exponents β, we want to discuss about the smallest and the largest angles that can be observed in Figure 4.23 and in Figure 4.39. A number of them arises from our approximation methods. When we get the "Shortest Path" graph, it may happen that the computed bifurcation points do not coincide

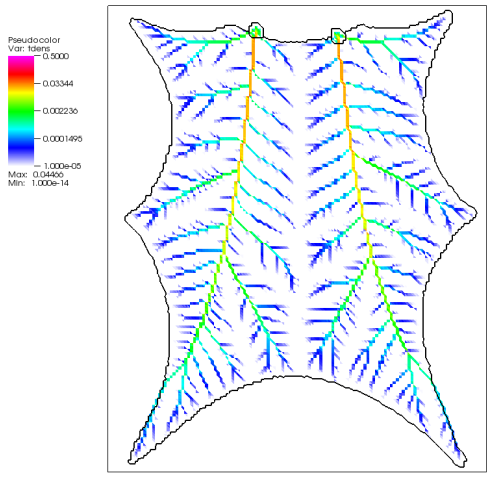

Figure 4.24: $\mu \in [10^{-5}, 0.5]$

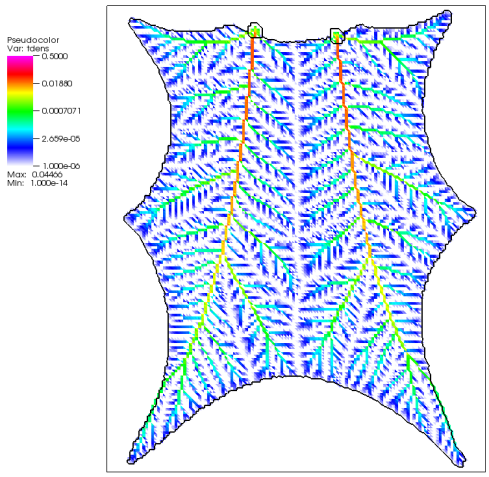

Figure 4.25: $\mu \in [10^{-6}, 0.5]$

Figure 4.26: Example of the solution μ for a fixed $\beta = 1.20$ for the refined mesh and different values of μ_{min}.

with the real bifurcation points, hence in these situations some small angles may arise. On the contrary, the largest angles arise when we join two near bifurcation points in the final step of our approximation method.

4.3 Analysis of numerical experiments

In the previous section we showed the results obtained for a fixed exponent $\beta = 1.20$. These results seem to have branching angles similar to Figure 4.1, so we decided to study mainly some cases in which $\beta \approx 1.20$, but firstly we would like to show a comparison of our results for $\beta = 1.20$ and $\beta = 1.40$ in order to show that the thesis of Lemma 9 holds. We are reporting only the solution μ (Figure 4.40) and the angles analysis for the non-refined mesh when $\beta = 1.40$. We can see the histogram for the angles in Figure 4.41.

Now we are going to compare the statistical data obtained for $\beta = 1.40$ with the data we shown in the previous section for $\beta = 1.20$. In 4.3 we can see how mean and median increased as β increased, so our experiments do not contradict Lemma 9.

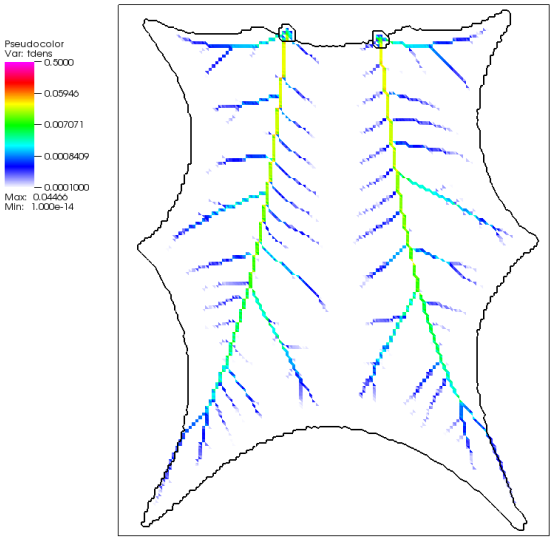

Figure 4.27: Solution μ when $\beta = 1.20$ and $\mu_{min} = 10^{-4}$ using a refined mesh.

β	Mean	Median	Variance	Skewness
1.20	55 ° 48'	54 ° 36'	355.68	0.82
1.40	68 ° 51'	74 ° 27'	598.36	0.21

Table 4.3: Comparison of the Statistical data on the angles for $\beta = 1.20$ and $\beta = 1.40$ when the non refined mesh has been used.

In Table 4.4 we show the statistical data for the angles for various exponent $\beta \in [1.15, 1.25]$. We can observe how basically the measures of the branching angles seem to increase as β increases, but there are some values, such as $\beta = 1.19$ that seem to contradict Lemma 9. But the errors we obtained are not too significant, so they may be caused by our approximation methods. This is the reason why we are going to show graphs and histograms obtained by the solution of DMK for the values of β analyzed in Table 4.4. We chose to report here the graphs because branching angles are more evident than in the solution μ of our problem. Moreover, we are considering the initial graphs in order to not consider the approximation errors of the reduced graphs.

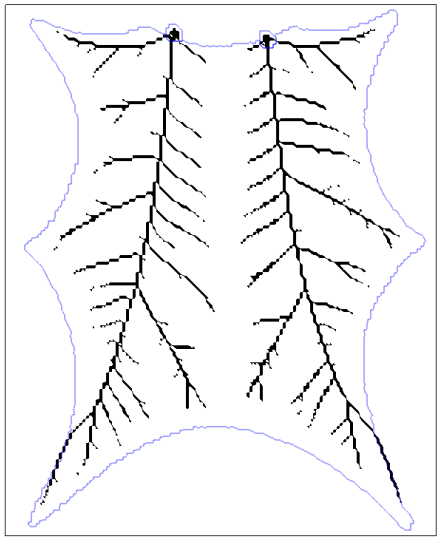

Figure 4.28: Graph for μ when $\beta = 1.20$ and $\mu_{min} = 10^{-4}$ using a refined mesh.

As we can observe in Figure 4.51 and in Figure 4.54, there is a number of obtuse angles, caused by our approximation methods, which distorts mean and median of Table 4.4 for $\beta = 1.19$. In general we can see how there are some numerical approximation angles (they can be easily observed from the histograms in Figure 4.44,Figure 4.47, Figure 4.50, Figure 4.53,Figure 4.50, Figure 4.59,Figure 4.62, Figure 4.65,Figure 4.68 and Figure 4.71), but they do not distort too much the statistical data in Table 4.4, as we can guess from the graphs in Figure 4.43, Figure 4.46, Figure 4.49, Figure 4.52, Figure 4.55, Figure 4.58, Figure 4.61, Figure 4.64, Figure 4.67 and Figure 4.70 so we are confident about our methods.

4.4 Final Considerations

As we observed in the previous sections, our numerical approach seem to approximate quite well Figure 4.2, if we ignore the loops that are visible in this figure. Moreover, our results seem to satisfy the theoretical relation between the exponent β and the measure of branching angles described by Lemma 9, so we are confident that, after some modifications, our method will be able to approximate Figure 4.2 even better.

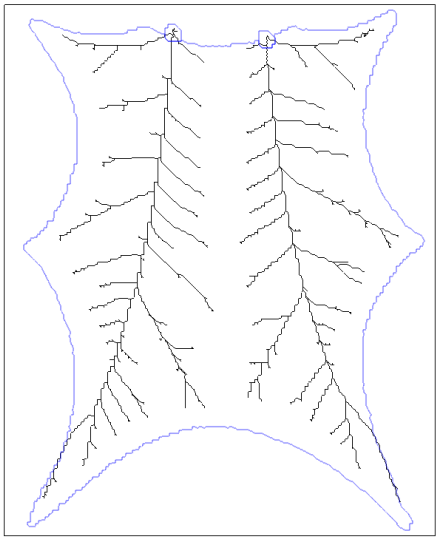

Figure 4.29: Shortest Path Graph for μ when $\beta = 1.20$ and $\mu_{min} = 10^{-4}$ using a refined mesh.

Finally, we think that we could be able also to find out which of the four optimality principles described in the biological literature in Chapter 2 rules our model. Indeed, we can easily obtain information about the measure and the position of a branching angle in our domain and Proposition 22 gives us a link between the known exponent β of Extended DMK model and the exponent x of the generalized Murray's Law (Equation (2.9)). So, if we were able to determine the radii ratio $\alpha = r_2/r_1 \in]0, 1[$, we could compare our numerical results with Woldenberg's theoretical biological results, described in Table 2.2. We conjecture that $(r_2/r_1)^4 = \mu_2/\mu_1$, where r_i indicates the radio of the i-th child vessel near a bifurcation and μ_i indicates its density. We have not done a sufficient number of numerical experiments, so we are not able to confirm our conjecture, but we are confident about it.
In conclusion, we think that, if we knew a periodic forcing function which can approximate well the heartbeat, we are confident that the results of our experiments will be even more similar to Figure 4.2.

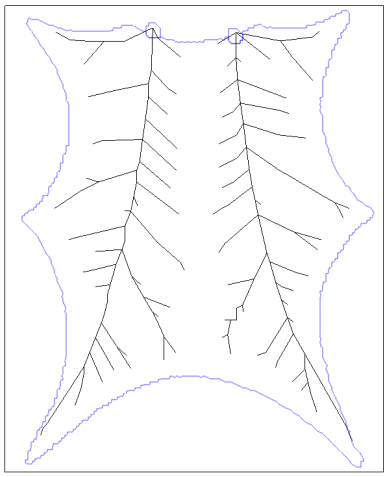

Figure 4.30: Reduced Graph with only sources, leaves and bifurcation points

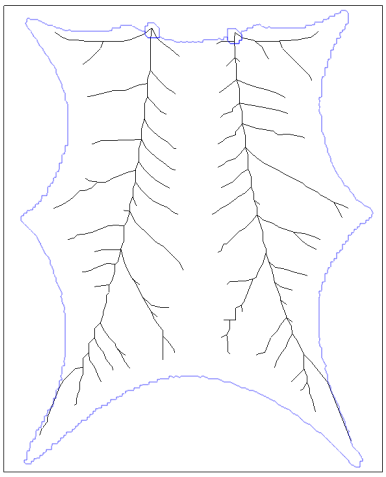

Figure 4.31: Reduced graph with Euclidean distance used for additional points.

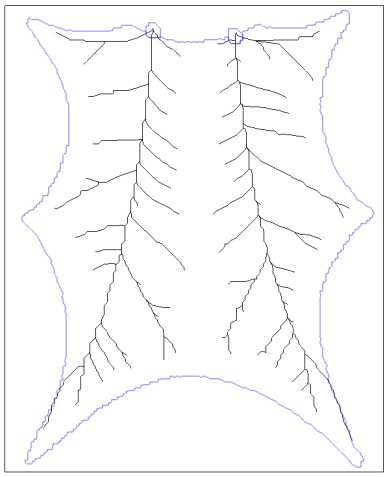

Figure 4.32: Reduced graph with graph distance used for additional points.

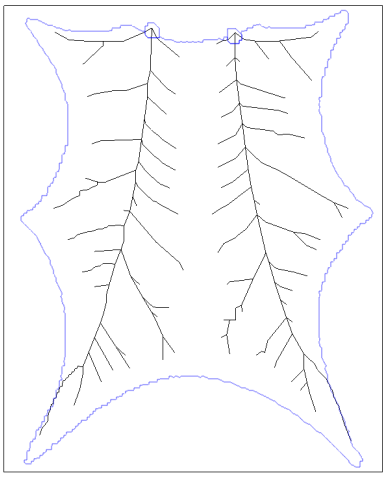

Figure 4.33: Reduced graph with security region used for additional points.

Figure 4.34: Application of the four different reduction methods for the "Shortest Path" Graph in Figure 4.29

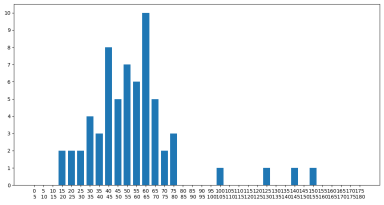

Figure 4.35: Histogram of the measure of the bifurcation angles for reduced Graph with only sources, leaves and bifurcation points (Figure 4.30).

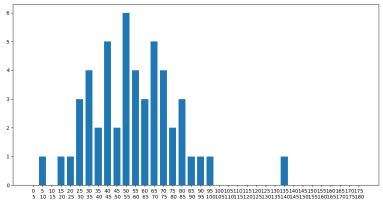

Figure 4.36: Histogram of the measure of the bifurcation angles for reduced graph with Euclidean distance used for additional points (Figure 4.31).

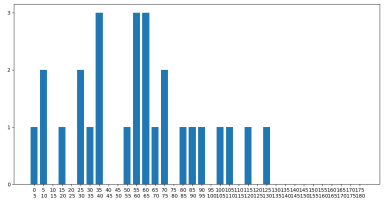

Figure 4.37: Histogram of the measure of the bifurcation angles for reduced graph with graph distance used for additional points (Figure 4.32).

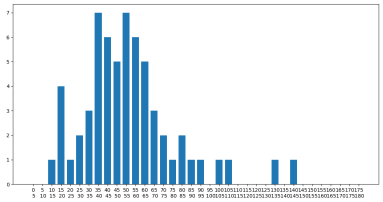

Figure 4.38: Histogram of the measure of the bifurcation angles for reduced graph with security region used for additional points (Figure 4.33).

Figure 4.39: Histograms of the measure of the bifurcation angles for the four different reduction methods for the "Shortest Path" Graph in Figure 4.29

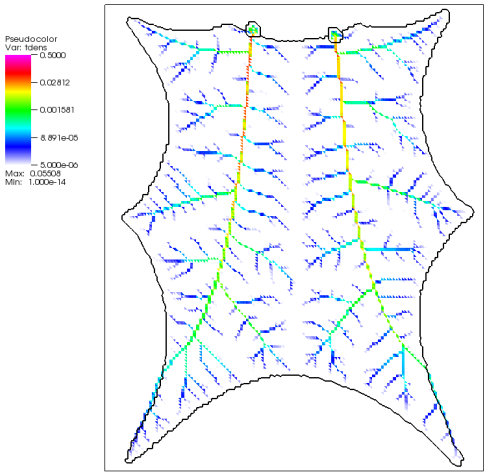

Figure 4.40: Solution for the non-refined mesh when $\mu \in [5 \cdot 10^{-5}, 0.5]$ and $\beta = 1.40$

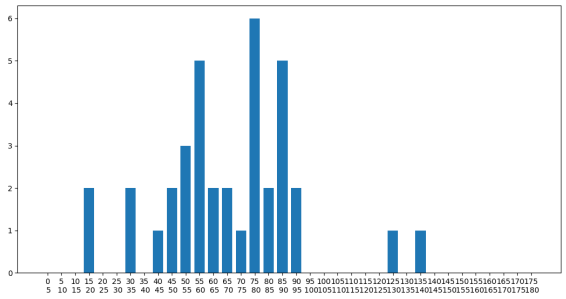

Figure 4.41: Histogram of the angles for $\beta = 1.40$

Figure 4.42: Solution and angles for the non-refined mesh when $\beta = 1.40$

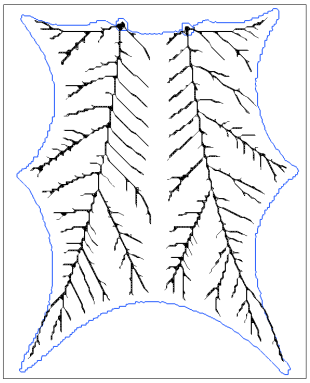

Figure 4.43: Solution for the non-refined mesh when $\mu \in [5 \cdot 10^{-5}, 0.5]$ and $\beta = 1.15$

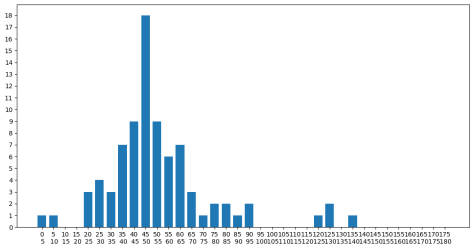

Figure 4.44: Histogram of the angles for $\beta = 1.15$

Figure 4.45: Solution and angles for the non-refined mesh when $\beta = 1.15$

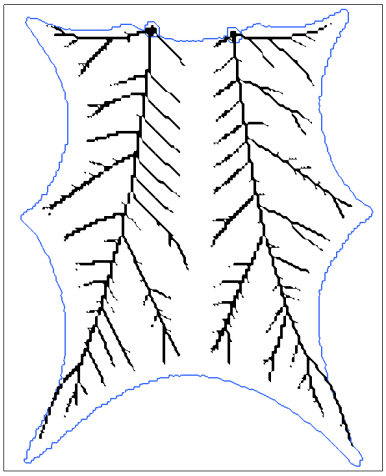

Figure 4.46: Solution for the refined mesh when $\mu \in [10^{-4}, 0.5]$ and $\beta = 1.15$

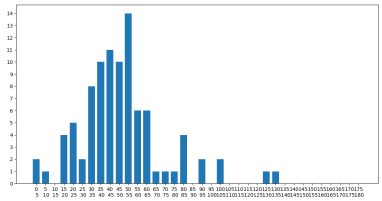

Figure 4.47: Histogram of the angles for $\beta = 1.15$

Figure 4.48: Solution and angles for the refined mesh when $\beta = 1.15$

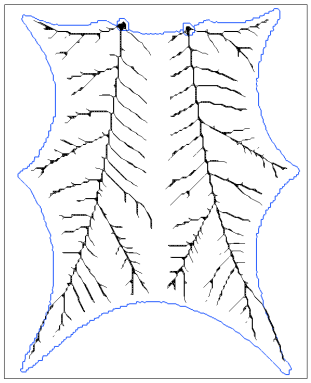

Figure 4.49: Solution for the non-refined mesh when $\mu \in [5 \cdot 10^{-5}, 0.5]$ and $\beta = 1.19$

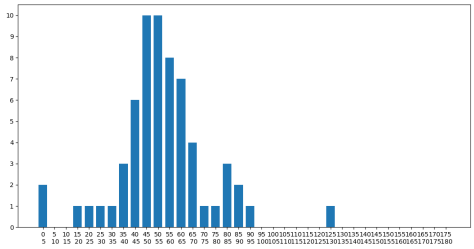

Figure 4.50: Histogram of the angles for $\beta = 1.19$

Figure 4.51: Solution and angles for the non-refined mesh when $\beta = 1.19$

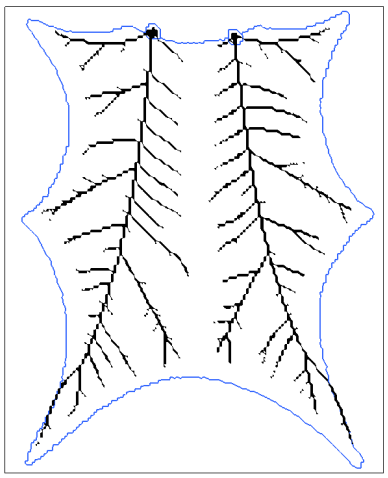

Figure 4.52: Solution for the refined mesh when $\mu \in [10^{-4}, 0.5]$ and $\beta = 1.19$

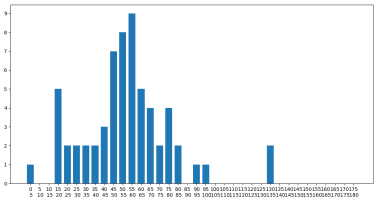

Figure 4.53: Histogram of the angles for $\beta = 1.19$

Figure 4.54: Solution and angles for the refined mesh when $\beta = 1.19$

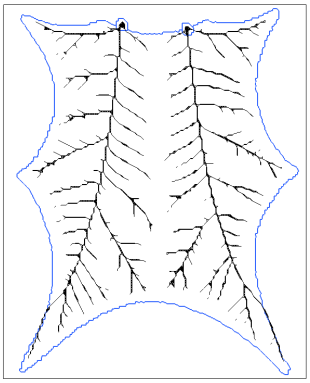

Figure 4.55: Solution for the non-refined mesh when $\mu \in [5 \cdot 10^{-5}, 0.5]$ and $\beta = 1.21$

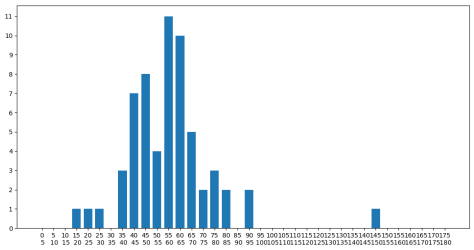

Figure 4.56: Histogram of the angles for $\beta = 1.21$

Figure 4.57: Solution and angles for the non-refined mesh when $\beta = 1.21$

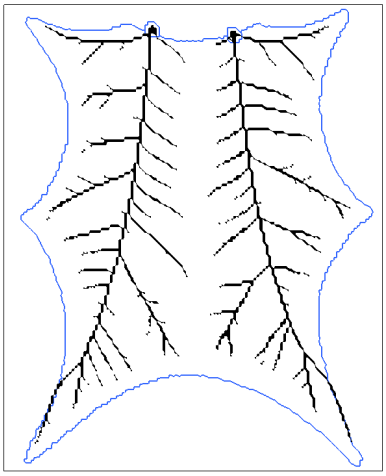

Figure 4.58: Solution for the refined mesh when $\mu \in [10^{-4}, 0.5]$ and $\beta = 1.21$

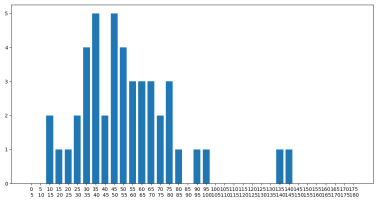

Figure 4.59: Histogram of the angles for $\beta = 1.21$

Figure 4.60: Solution and angles for the refined mesh when $\beta = 1.21$

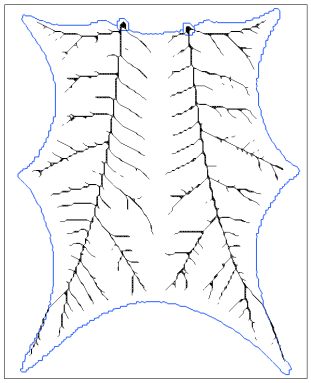

Figure 4.61: Solution for the non-refined mesh when $\mu \in [5 \cdot 10^{-5}, 0.5]$ and $\beta = 1.23$

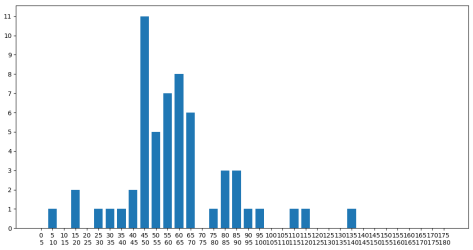

Figure 4.62: Histogram of the angles for $\beta = 1.23$

Figure 4.63: Solution and angles for the non-refined mesh when $\beta = 1.23$

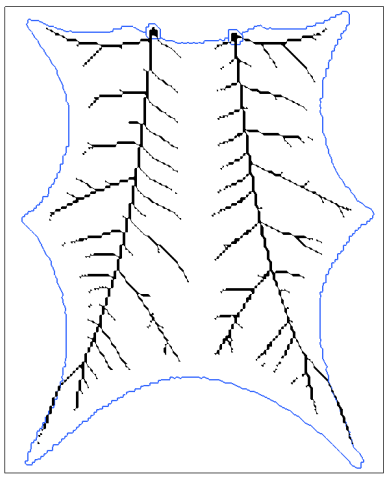

Figure 4.64: Solution for the refined mesh when $\mu \in [10^{-4}, 0.5]$ and $\beta = 1.23$

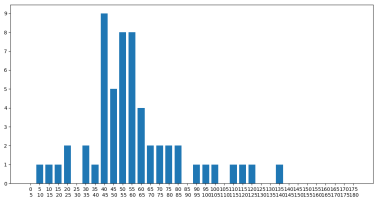

Figure 4.65: Histogram of the angles for $\beta = 1.23$

Figure 4.66: Solution and angles for the refined mesh when $\beta = 1.23$

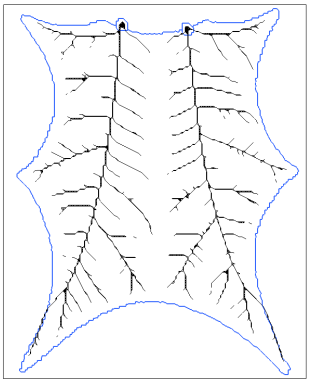

Figure 4.67: Solution for the non-refined mesh when $\mu \in [5 \cdot 10^{-5}, 0.5]$ and $\beta = 1.25$

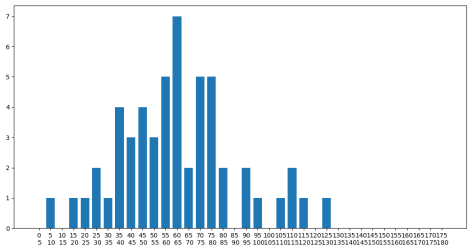

Figure 4.68: Histogram of the angles for $\beta = 1.25$

Figure 4.69: Solution and angles for the non-refined mesh when $\beta = 1.25$

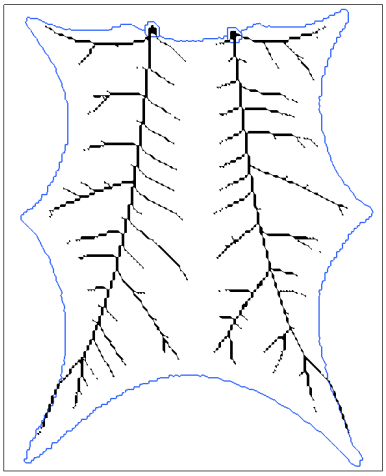

Figure 4.70: Solution for the refined mesh when $\mu \in [10^{-4}, 0.5]$ and $\beta = 1.25$

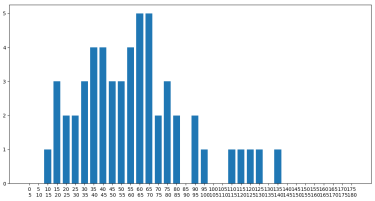

Figure 4.71: Histogram of the angles for $\beta = 1.25$

Figure 4.72: Solution and angles for the refined mesh when $\beta = 1.25$

β	Mean		Median		Variance		Skewness	
Ref	0	1	0	1	0	1	0	1
1.15	53 ° 30’	49 ° 00’	49 ° 39’	46 ° 57’	517.17	528.50	1.43	1.08
1.19	55 ° 57’	55 ° 36’	54 ° 39’	54 ° 51’	415.41	641.86	0.24	0.80
1.20	55 ° 48’	54 ° 39’	54 ° 36’	51 ° 21’	355.68	638.63	0.82	1.21
1.21	60 ° 54’	58 ° 21’	58 ° 39’	57 ° 06’	566.28	648.83	0.99	0.70
1.23	61 ° 09’	58 ° 00’	57 ° 06’	52 ° 09’	488.84	650.85	0.80	0.94
1.25	62 ° 51’	59 ° 06’	61 ° 30’	58 ° 09’	628.11	842.54	0.46	0.72

Table 4.4: Comparison of the Statistical data on the angles for different values of β.

Bibliography

[1] L. Bergamaschi, E. Facca, A. Martinez, and M. Putti, *Spectral preconditioners for the efficient numerical solution of a continuous branched transport model*, Journal of Computational and Applied Mathematics, (2018).

[2] M. Bernot, V. Caselles, and J.-M. Morel, *Traffic plans*, Publicacions Matemàtiques, 49(2) (2005), pp. 417–451.

[3] M. Bernot, V. Caselles, and J.-M. Morel, *Optimal Transportation Networks*, vol. 1955 of Lecture Notes in Mathematics, Springer, 2009.

[4] L. Berti, *Dynamic monge-kantovorich equations on surfaces with applications to purkinje network and cut loci*, Master's thesis, Università degli Studi di Padova.

[5] BogoToBogo, *Dijkstra's shortest path algorithm.*

[6] V. Bonifaci, K. Mehlhorn, and G. Varma, *Physarum can compute shortest paths*, Journal of theoretical Biology, 309 (2012), pp. 121–133.

[7] G. Bouchitté and G. Buttazzo, *Shape optimization solutions via monge-kantorovich equation*, CR Math, 324 (1997), pp. 1185–1191.

[8] M. A. Changizi and C. Cherniak, *Modeling the large-scale geometry of human coronary arteries*, Canadian Journal of Physiology and Pharmacology, 78 (2000), pp. 603–611.

[9] J. F. Cohnheim, *Untersuchungen über die embolischen process*, (1872).

[10] P. S. Doods, D. H. Rothman, and D. S. Weitz, *Re-examination of the "3/4-law" of metabolism*, Journal of Theoretical Biology, 209 (2001), pp. 9–27.

[11] L. C. Evans and W. Gangbo, *Differential equations methods for the monge-kantorovich mass transfer problem*, American Mathematical Society, 653 (1999).

[12] E. Facca, *Biological Inspired Formulation of Optimal Transport Problem*, PhD thesis, Università degli Studi di Padova.

[13] E. Facca, F. Cardin, and M. Putti, *A continuous model of slime mold dynamics*, SIAM Journal of Applied Mathematics, (2017).

[14] E. Facca, S. Daneri, F. Cardin, and M. Putti, *Numerical solution of monge-kantorovich equations via a dynamic formulation*, SIAM Journal of Applied Mathematics, (2017).

[15] E. N. Gilbert, *Minimum cost communication networks*, Bells Labs Technical Joournal, 46 (1967), pp. 2209–2227.

[16] J. A. Harris and F. G. Benedict, *A biometric study of basal metabolism in man*, Carnegie Institute of Washington Publications, 279 (1919), pp. 1–266.

[17] W. R. Hess, *Über die periphere regulierung der blutzirkulation*, Pflügers Archiv European Journal of Physiology, 168 (1917), pp. 439–490.

[18] H. Kitaoka, R. I. Takaki, and B. Suji, *A three-dimensional model of the human airway tree*, The American Physiological Society, (1999), pp. 2207–2217.

[19] M. Kleiber, *Body size and metabolism*, Hilgardia, A Journal of Agricultural Science, 6 (January 1932), pp. 315–353.

[20] F. Maddalena and S. Solimini, *A variational model of irrigation patterns*, Interfaces and Free Boundaries, 5(4) (2003), pp. 391–416.

[21] G. Monge, *Mémoire sur la théorie des déblais et des remblais*, De l'Imprimerie Royale, (1781).

[22] C. D. Murray, *The physiological principle of minimum work applied to the angle of branching of arteries*, The Journal of General Physiology, (April 1926), pp. 835–841.

[23] ——, *The physiological principle of minimum work*, Proceedings of the National Academy of Sciences, 12 (January 1926), pp. 207–214.

[24] F. Santambrogio, *Optimal transport for applied mathematicians*, Birkäuser, (2015).

[25] L. A. Taber, S. Ng, A. M. Quesnel, J. Whatman, and C. J. Carmen, *Investigating murray's law in the chick embryo*, Journal of Biomechanics, 34 (2001), pp. 121–124.

[26] C. A. Taylor, T. A. Fonte, and J. K. Min, *Computational fluid dynamics applied to cardiac computed tomography for noninvasive quantification of fractional flow reserve*, Journal of the American College of Cardiology, 61 (June 2013), pp. 2233–2241.

[27] A. Tero, R. Kobayashi, and T. Nakagaki, *A mathematical model for adaptive transport network in path finding by true slime mold*, Journal of theoretical Biology, 244 (2007), pp. 553–564.

[28] R. Tosi, *Numerical solution of the three dimensional optimal transport problem*, Master's thesis, Università degli Studi di Padova.

[29] H. Uylings, *Optimization of diameters and bifurcation angles in lung and vascular tree structures*, Bulletin of Mathematical Biology, 39 (1977), pp. 509–519.

[30] G. B. West, J. H. Brown, and B. J. Enquist, *A general model for the origin of allometric scaling laws in biology*, Science Magazine, 276 (4 April 1997), pp. 122–127.

[31] M. J. Woldenberg and K. Horsfield, *Finding the optimal lengths for three branches at a junction*, Journal of theoretical Biology, 104 (1983), pp. 301–318.

[32] ——, *Relation of branching angles to optimality for four cost principles*, Journal of theoretical Biology, 122 (1986), pp. 187–204.

[33] Q. Xia, *Optimal paths related to transport problems*, Communications in Contemporary Mathematics, 5 (2003), pp. 251–279.

[34] M. Zamir, *Optimality in arterial branching*, Journal of theoretical Biology, 62 (1976), pp. 227–251.

[35] ——, *Arterial bifurcations in the cardiovascular system of a rat*, The Journal of General Physiology, 81 (March 1983), pp. 325–335.